Effect of Stochastic Loading on Tensile Damage and Fracture of Fiber-Reinforced Ceramic-Matrix Composites

Longbiao Li

College of Civil Aviation, Nanjing University of Aeronautics and Astronautics, No.29 Yudao St., Nanjing 210016, China; llb451@nuaa.edu.cn

Abstract: In this paper, the effect of stochastic loading on tensile damage and fracture of fiber-reinforced ceramic-matrix composites (CMCs) is investigated. A micromechanical constitutive model is developed considering multiple damage mechanisms under tensile loading. The relationship between stochastic stress, tangent modulus, interface debonding and fiber broken is established. The effects of the fiber volume, interface shear stress, interface debonding energy, saturation matrix crack spacing and fiber strength on tensile stress–strain curve, tangent modulus, interface debonding fraction and fiber broken fraction are analyzed. The experimental tensile damage and fracture of unidirectional and 2D SiC/SiC composites subjected to different stochastic loading stress are predicted. When fiber volume increases, the initial composite strain decreases, the initial tangent modulus increases, the transition stress for interface debonding decreases and the initial fiber broken fraction decreases. When fiber strength increases, the initial composite strain and fiber broken fraction decrease.

Keywords: ceramic-matrix composites (CMCs); Stochastic loading; tensile; matrix cracking; interface debonding; fiber failure

---

1. Introduction

Ceramic-matrix composites (CMCs) have the advantages of high-temperature resistance, corrosion resistance, low density, high specific strength and high specific modulus [1]. The fabrication methods of CMCs include the chemical vapor infiltration (CVI), polymer infiltration and pyrolysis process (PIP) and melt infiltration (MI). The mechanical performance of CMCs depends on the fabrication method. To ensure the reliability and safety of fiber-reinforced CMCs used in hot-section components of an aero engine, it is necessary to develop performance evaluation, damage evolution, strength and life prediction tools for airworthiness certification [2]. Since the applications of fiber-reinforced CMCs involve components with lives that are measured in tens of thousands of hours, the successful design and implementation of CMC components depend on the knowledge of the material behavior over periods of time comparable to the expected service life of the component [3].

Under tensile loading, multiple damage mechanisms of matrix cracking, interface debonding and fiber failure occur [4–8]. The tensile stress–strain curves can be divided into four stages, including:

(1) Stage I, linear-elastic region.
(2) Stage II, matrix cracking and interface debonding region. Matrix micro cracking occurs first and the fiber debonding from the matrix, leading to nonlinear behavior of CMCs.
(3) Stage III, saturation matrix cracking region. Matrix cracking approaches saturation with complete debonding of the fiber from the matrix.
(4) Stage IV, fiber failure region. The fiber gradually fractures with increasing applied stress.

The composite elastic modulus, proportional limit stress, ultimate tensile strength and the fracture strain can be obtained from the tensile stress–strain curve. For the SiC/SiC composite fabricated using the MI method, the fracture strength and strain of Hi-Nicalon S SiC/SiC composite is much higher than that of Tyranno SA3 SiC/SiC composite; however, the initial elastic modulus and proportional limit stress of Hi-Nicalon S SiC/SiC composite is lower than that of Tyranno SA3 SiC/SiC composite at the same fiber volume of 34.8% and the composite tensile strength increases with the fiber volume [9]. Marshall et al. [10] and Zok and Spearing [11] investigated the first matrix cracking and matrix multiple cracking evolution in fiber-reinforced CMCs using the fracture mechanics approach. Curtin [12] investigated multiple matrix cracking evolution of CMCs considering matrix internal flaws. Evans [13] developed an approach for design and life prediction issues for fiber-reinforced CMCs and established the relationship between macro mechanical behavior and constituent properties of CMCs. McNulty and Zok [14] investigated the low-cycle fatigue damage mechanism and established the damage models for predicting the low-cycle fatigue life of CMCs. Naslain et al. [15] investigated the monotonic and cyclic tensile behavior of Nicalon™ SiC/SiC minicomposite at room temperature. The relationship between the statistical parameters of both the fiber and the matrix and the fiber/matrix interfacial parameters and the effect of environment and the tensile curves has been established. Goto and Kagawa [16] investigated the tensile and fracture behavior of a bi-directional woven Nicalon™ SiC/SiC composite at room temperature. The tensile stress–strain curve shows nonlinear behavior above 70 MPa and the composite effective Young's modulus at fracture was about 40% of the initial value. Guo and Kagawa [6] investigated the tensile fracture behavior and tensile mechanical properties of Nicalon™ and Hi-Nicalon™ SiC/BN/SiC composites at temperature between 298 and 1400 K in air atmosphere. The tensile strength dropped from 140 MPa at 800 K to 41 MPa at 1200 K. Meyer and Waas [17] investigated tensile response of notched SiC/SiC composite at elevated temperature using a novel digital image correlation technique. Li et al. [18–20] developed a micromechanical approach to predict the tensile behavior of unidirectional, cross-ply, 2D and 2.5D woven CMCs considering the damage mechanisms of matrix cracking, interface debonding and fiber failure. However, the effect of stochastic loading on tensile damage and fracture of fiber-reinforced CMCs has not been investigated.

The objective of this paper is to investigate the effect of stochastic loading on tensile damage and fracture of fiber-reinforced CMCs for the first time. A micromechanical constitutive model is developed considering multiple damage mechanisms under tensile loading. The relationship between stochastic stress, tangent modulus, interface debonding and fiber broken is established. The effects of fiber volume, interface shear stress, interface debonding energy, saturation matrix crack spacing and fiber strength on tensile stress–strain curve, tangent modulus, interface debonding fraction and fiber broken fraction are analyzed. The experimental tensile damage and fracture of unidirectional and 2D SiC/SiC composites subjected to different stochastic loading stress are predicted.

2. Theoretical Model

When stochastic stress occurs under tensile loading, matrix cracking, interface debonding, and fiber failure occur. Multiple stochastic loading sequence is shown in Figure 1. The shear-lag model is used to analyze micro stress filed of damaged composite. A unit cell is extracted from the ceramic composite system, as shown in Figure 2. The fiber axial stress in different damage regions is given by Equation (1).

$$\sigma_{\rm f}(x) = \begin{cases} \Phi - \frac{2\tau_{\rm i}}{r_{\rm f}}x, x \in [0, l_{\rm d}] \\ \sigma_{\rm fo} + \left(\Phi - \sigma_{\rm fo} - 2\frac{l_{\rm d}}{r_{\rm f}}\tau_{\rm i}\right)\exp\left(-\rho\frac{x-l_{\rm d}}{r_{\rm f}}\right), x \in \left[l_{\rm d}, \frac{l_{\rm c}}{2}\right] \end{cases} \tag{1}$$

where Φ is the fiber intact stress, $\tau_{\rm i}$ is the interface shear stress, $r_{\rm f}$ is the fiber radius, $\sigma_{\rm fo}$ is the fiber axial stress in the interface bonding region, $l_{\rm d}$ is the interface debonding length, $l_{\rm c}$ is the matrix crack spacing and ρ is the shear-lag model parameter.
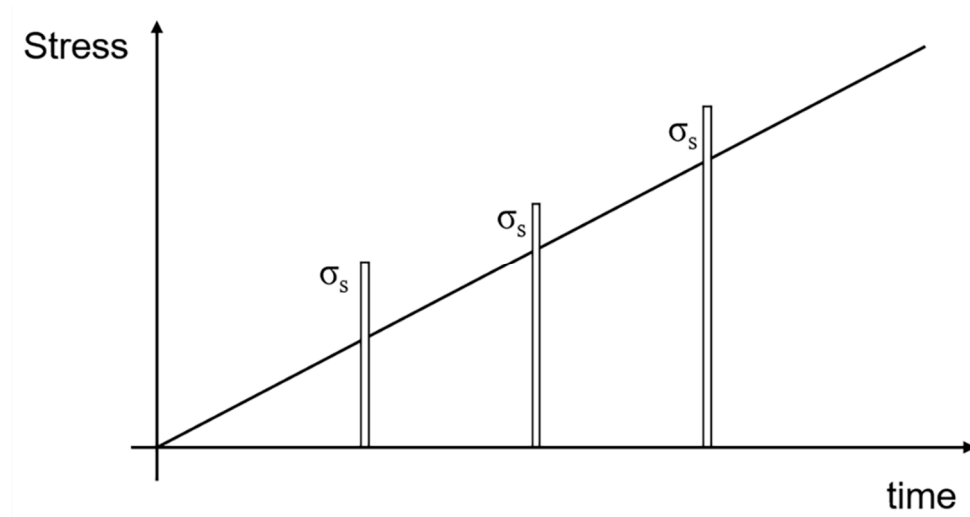
Figure 1. The diagram of stochastic loading under tensile loading.
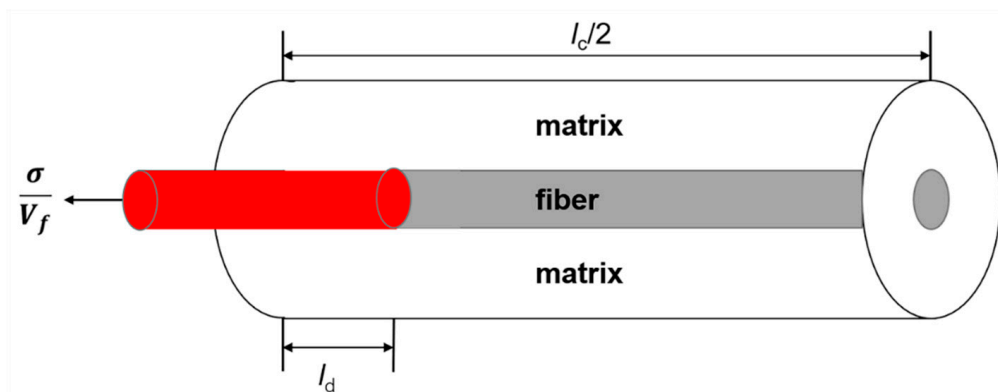
Figure 2. The unit cell of damaged composite.

Using stochastic matrix cracking model, the relationship between stochastic stress and matrix crack spacing is given by Equation (2) [12].

$$l_c = l_s \left\{ 1 - \exp\left[-\left(\frac{\sigma_m}{\sigma_R} \right)^m \right] \right\}^{-1} \tag{2}$$

where l_s is the saturation matrix crack spacing, σ_m is the matrix stress, σ_R is matrix cracking characteristic stress and m is the matrix Weibull modulus.

The fracture mechanics approach is used to determine the fiber/matrix interface debonding length. The interface debonding length is determined by Equation (3).

$$l_d = \frac{r_f}{2} \left(\frac{V_m E_m \sigma}{V_f E_c \tau_i} - \frac{1}{\rho} \right) - \sqrt{ \left(\frac{r_f}{2\rho} \right)^2 + \frac{r_f V_m E_m E_f}{E_c \tau_i^2} \zeta_d } \tag{3}$$

where V_f and V_m are the fiber and matrix volume fraction, respectively, E_m and E_c are the matrix and composite elastic modulus, respectively, and ζ_d is the interface debonding energy.

The Global Load Sharing (GLS) criterion is used to determine the intact fiber stress. The relationship between the fiber intact stress, fiber failure probability and fiber pullout length is given by Equation (4) [21].

$$\frac{\sigma}{V_f} = \Phi(1 - P(\Phi)) + \frac{2\tau_i}{r_f} \langle L \rangle P(\Phi) \tag{4}$$

where $<L>$ is the average fiber pullout length, and $P(\Phi)$ is the fiber failure probability, which is obtained by Equation (5).

$$P(\Phi) = 1 - \exp\left[-\left(\frac{\Phi}{\sigma_c}\right)^{m_f+1}\right] \tag{5}$$

where σ_c is the fiber characteristic strength, and m_f is the fiber Weibull modulus.

When matrix cracking and interface debonding occur, the composite strain is given by Equation (6).

$$\varepsilon_c = \begin{cases} \frac{\sigma}{V_f E_f}\eta - \frac{\tau_i}{E_f}\frac{l_d}{r_f}\eta + \frac{\sigma_{fo}}{E_f}(1-\eta) - \frac{2}{\rho E_f}\left(\frac{V_m}{V_f}\frac{r_f}{l_c}\sigma_{mo} - \eta\tau_i\right) \\ \qquad \times\left[\exp\left(-\frac{\rho}{2}\frac{l_c}{r_f}(1-\eta)\right) - 1\right] - (\alpha_c - \alpha_f)\Delta T, \eta < 1 \\ \frac{\sigma}{V_f E_f} - \frac{1}{2}\frac{\tau_i}{E_f}\frac{l_c}{r_f} - (\alpha_c - \alpha_f)\Delta T, \eta = 1 \end{cases} \tag{6}$$

When fiber failure occurs, the composite strain is given by Equation (7).

$$\varepsilon_c = \begin{cases} \frac{\Phi}{E_f}\eta - \frac{\tau_i}{E_f}\frac{l_d}{r_f}\eta + \frac{\sigma_{fo}}{E_f}(1-\eta) - \frac{2}{\rho E_f}\left(\frac{r_f}{l_c}(\Phi - \sigma_{fo}) - \eta\tau_i\right) \\ \qquad \times\left[\exp\left(-\frac{\rho}{2}\frac{l_c}{r_f}(1-\eta)\right) - 1\right] - (\alpha_c - \alpha_f)\Delta T, \eta < 1 \\ \frac{\Phi}{E_f} - \frac{1}{2}\frac{\tau_i}{E_f}\frac{l_c}{r_f} - (\alpha_c - \alpha_f)\Delta T, \eta = 1 \end{cases} \tag{7}$$

where η is the interface debonding fraction, as shown in Equation (8).

$$\eta = 2\frac{l_d}{l_c} \tag{8}$$

The tangent modulus is defined by Equation (9).

$$E_p = \frac{d\sigma}{d\varepsilon} \tag{9}$$

3. Results and Discussion

Under stochastic loading, the damages of the matrix cracking, interface debonding and fiber failure occur. The micro stress filed of the damaged CMCs after stochastic loading is given by Equation (1). The fiber axial stress distribution is affected by the stochastic loading stress level, matrix cracking, interface debonding and fiber failure. The stochastic matrix cracking model is used to determine the matrix crack spacing at the applied stress level, as shown in Equation (2), and the fracture mechanics interface debonding criterion is used to determine the interface debonding length, and the GLS criterion is used to determine the load allocation between fracture and intact fibers. The micromechanical constitutive models for the conditions of the matrix cracking, interface debonding and fiber failure are given by Equations (6) and (7). Using the developed micromechanicam constitutive models and damage models, the effects of the fiber volume, interface shear stress, interface debonding energy, matrix crack spacing and fiber strength on tensile stress–strain curve, tangent modulus, interface debonding fraction and fiber broken fraction of SiC/SiC composite subjected to different stochastic loading are analyzed. Li et al. [4] investigated the tensile behavior of 2D woven SiC/SiC composite at room temperature. The composite was fabricated using the CVI method with the PyC interphase. The tensile experiments were conducted under displacement contrl of 0.3 mm/min. The material properties are given by: $V_f = 0.2$, $E_f = 350$ GPa, $E_m = 300$ GPa, $r_f = 7.5$ μm, $\alpha_f = 4.0 \times 10^{-6}$/°C, $\alpha_m = 4.8 \times 10^{-6}$/°C, $\Delta T = -1000$ °C, $\zeta_d = 0.5$ J/m^2, $\tau_i = 25$ MPa and $m_f = 3$.

3.1. Effect of Fiber Volume on Tensile Damage and Fracture of SiC/SiC Composite with Stochastic Loading

The fiber volume affects the tensile behavior of CMCs. The fiber volume range of SiC/SiC composite is between V_f = 27.7 and 40% [9]. In the present analysis, the effect of the fiber volume (i.e., V_f = 0.3 and 0.35) on the tensile stress–strain curves, tangent modulus, interface debonding fraction and broken fiber fraction of SiC/SiC composite subjected to the stochastic loading of σ_s = 200, 300 and 350 MPa are shown in Figure 3; Figure 4 and Table 1. When the fiber volume increases, the stress carried by the fiber increases, the initial composite strain decreases, the initial tangent modulus increases, the transition stress for the interface debonding decreases and the initial fiber broken fraction decreases.
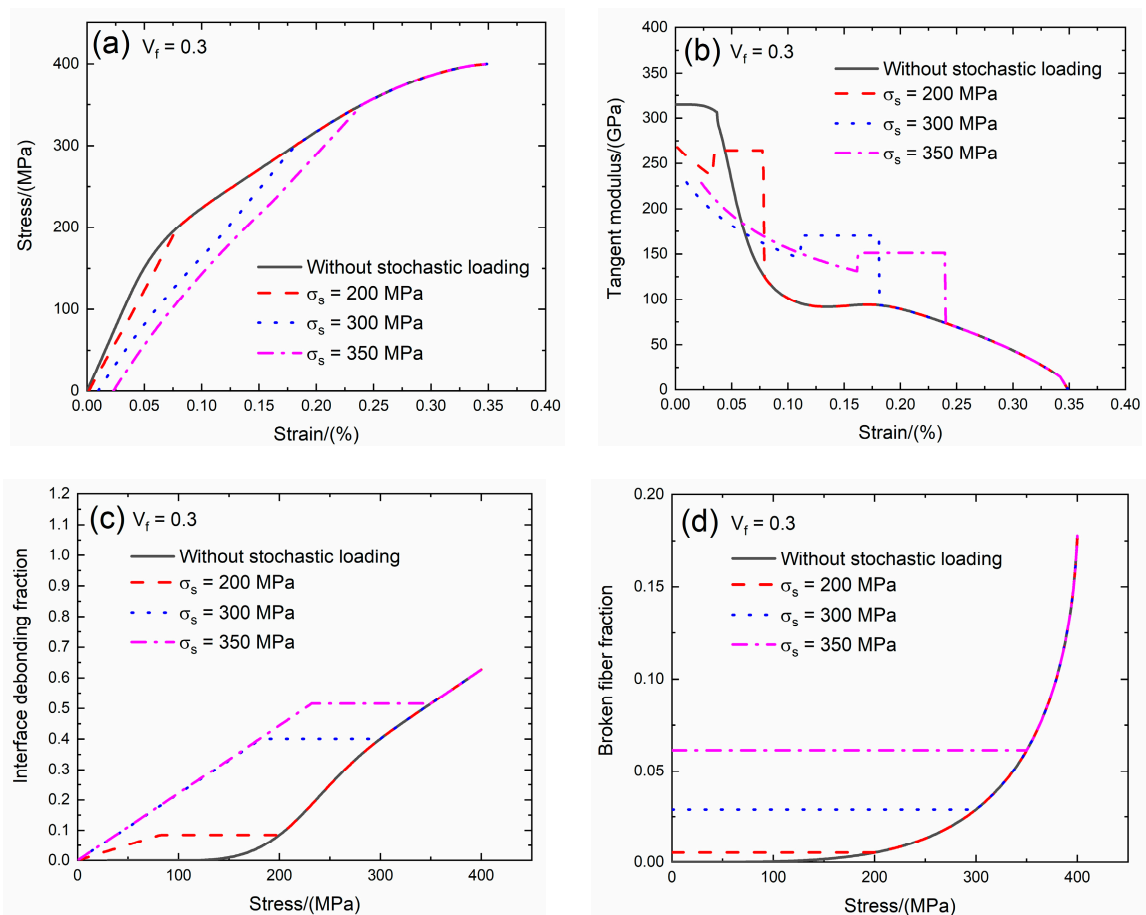
Figure 3. (**a**) The tensile stress–strain curves; (**b**) the tangent modulus versus strain curves; (**c**) the interface debonding fraction versus stress curves; and (**d**) the broken fibers fraction versus stress curves of SiC/SiC composite for conditions without stochastic loading and with stochastic loading of σ_s = 200, 300 and 350 MPa when V_f = 0.3.
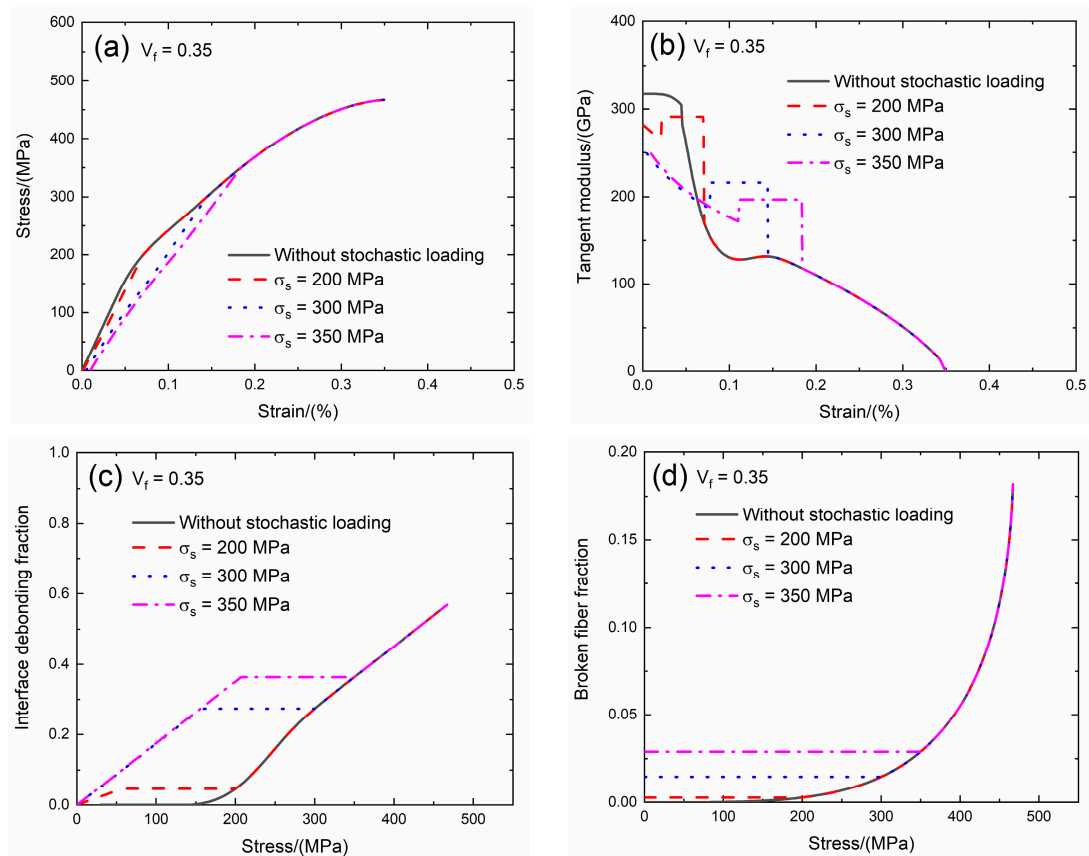
Figure 4. (**a**) The tensile stress–strain curves; (**b**) the tangent modulus versus strain curves; (**c**) the interface debonding fraction versus stress curves; and (**d**) the broken fibers fraction versus stress curves of SiC/SiC composite for conditions without stochastic loading and with stochastic loading of σ_s = 200, 300 and 350 MPa when V_f = 0.35.

Table 1. The effect of the fiber volume (V_f = 0.3 and 0.35) on tensile stress–strain curve, tangent modulus, interface debonding fraction and broken fiber fraction of SiC/SiC composite subjected to stochastic loading of σ_s = 200, 300 and 350 MPa.

	ε_0/(%)	E_p/(GPa)	σ_{tr}/(MPa)	P/(%)
	σ_s = 200 MPa			
	0.00161	268	79.2	0.005
V_f = 0.3	σ_s = 300 MPa			
	0.0098	229	178.2	0.028
	σ_s = 350 MPa			
	0.023	228	231	0.060
	σ_s = 200 MPa			
	0.0009	281	55	0.0027
V_f = 0.35	σ_s = 300 MPa			
	0.0047	249	156.2	0.014
	σ_s = 350 MPa			
	0.0095	248	206.8	0.028

When $V_f = 0.3$ under $\sigma_s = 200$ MPa, the damages of matrix cracking and interface debonding occur at $\sigma_s = 200$ MPa, leading to the increase of the composite initial strain, decreasing of the tangent modulus and increase of the broken fiber fraction. The initial composite strain is $\varepsilon_0 = 0.00161\%$ due to the matrix cracking and interface debonding at $\sigma_s = 200$ MPa; the initial tangent modulus is $E_p = 268$ GPa, the degradation rate of the tangent modulus is 15% compared with the original specimen and the fiber broken fraction is $P = 0.005$. With increasing stress to $\sigma_{tr} = 79.2$ MPa, the interface debonding fraction increases, the tangent modulus decreases to $E_p = 235$ GPa corresponding to $\eta = 0.081$. Upon increasing stress from $\sigma_{tr} = 79.2$ MPa to $\sigma = 200$ MPa, the tangent modulus remains constant of $E_p = 264$ GPa with $\eta = 0.084$.

Under $\sigma_s = 300$ MPa, the initial composite strain is $\varepsilon_0 = 0.00982\%$ due to the damages of the matrix cracking and interface debonding at $\sigma_s = 300$ MPa; the initial tangent modulus is $E_p = 229$ GPa, the degradation rate of tangent modulus is 28% compared with the original specimen and the fiber broken fraction is $P = 0.028$. With increasing stress to $\sigma_{tr} = 178.2$ MPa, the interface debonding fraction increases, the tangent modulus decreases to $E_p = 145$ GPa corresponding to $\eta = 0.392$. Upon increasing stress from $\sigma_{tr} = 178.2$ MPa to $\sigma = 300$ MPa, the tangent modulus remains constant of $E_p = 170.1$ GPa with $\eta = 0.4$.

Under $\sigma_s = 350$ MPa, the initial composite strain is $\varepsilon_0 = 0.023\%$ due to the damages of the matrix cracking and interface debonding at $\sigma_s = 350$ MPa; the initial tangent modulus is $E_p = 228$ GPa, the degradation rate of tangent modulus is 28% compared with the original specimen and the fiber broken fraction is $P = 0.06$. With increasing stress to $\sigma_{tr} = 231$ MPa, the interface debonding fraction increases, the tangent modulus decreases to $E_p = 131$ GPa corresponding to $\eta = 0.51$. Upon increasing stress from $\sigma_{tr} = 131$ MPa to $\sigma = 350$ MPa, the tangent modulus remains constant of $E_p = 151$ GPa with $\eta = 0.51$.

When $V_f = 0.35$ under $\sigma_s = 200$ MPa, the damages of matrix cracking and interface debonding occur at $\sigma_s = 200$ MPa, leading to the increase of the composite initial strain, decreasing of the tangent modulus and increase of the broken fiber fraction. The initial composite strain is $\varepsilon_0 = 0.0009\%$; the initial tangent modulus is $E_p = 281$ GPa, the degradation rate of tangent modulus is 12% compared with original specimen and the fiber broken fraction is $P = 0.0027$. With increasing stress to $\sigma_{tr} = 55$ MPa, the interface debonding fraction increases, the tangent modulus decreases to $E_p = 265$ GPa corresponding to $\eta = 0.046$. Upon increasing stress from $\sigma_{tr} = 55$ MPa to $\sigma = 200$ MPa, the tangent modulus remains constant of $E_p = 291$ GPa with $\eta = 0.046$.

Under $\sigma_s = 300$ MPa, the initial composite strain is $\varepsilon_0 = 0.0047\%$ due to the damages of matrix cracking and interface debonding at $\sigma_s = 300$ MPa; the initial tangent modulus is $E_p = 249$ GPa, the degradation rate of tangent modulus is 22% compared with original specimen and the fiber broken fraction is $P = 0.014$. With increasing stress to $\sigma_{tr} = 156.2$ MPa, the interface debonding fraction increases and the tangent modulus decreases to $E_p = 201$ GPa corresponding to $\eta = 0.27$. When the stress increases from $\sigma_{tr} = 156.2$ MPa to $\sigma = 250$ MPa, the tangent modulus remains constant of $E_p = 216$ GPa with $\eta = 0.27$.

Under $\sigma_s = 350$ MPa, the initial composite strain is $\varepsilon_0 = 0.0095\%$ due to the damages of the matrix cracking and interface debonding at $\sigma_s = 350$ MPa; the initial tangent modulus is $E_p = 248$ GPa, the degradation rate of tangent modulus is 22% compared with original specimen and the fiber broken fraction is $P = 0.028$. With increasing stress to $\sigma_{tr} = 206.8$ MPa, the interface debonding fraction increases and the tangent modulus decreases to $E_p = 191.9$ GPa corresponding to the interface debonding fraction $\eta = 0.362$. When the stress increases from $\sigma_{tr} = 206.8$ MPa to $\sigma = 300$ MPa, the tangent modulus remains constant of $E_p = 196.7$ GPa with $\eta = 0.363$.

3.2. Effect of Interface Shear Stress on Tensile Damage and Fracture of SiC/SiC Composite with Stochastic Loading

The interface shear stress transfers the load between the fiber and the matrix when the matrix cracking and interface debonding occur. For the weak interface bonding between the fiber and the

matrix of SiC/SiC composite, the value of the interface shear stress is between τ_i = 10 and 30 MPa [22]. In the present analysis, the effect of the interface shear stress (i.e., τ_i = 15 and 20 MPa) on the tensile stress–strain curves, tangent modulus, interface debonding fraction and broken fiber fraction of SiC/SiC composite subjected to stochastic loading of σ_s = 200, 230 and 250 MPa are shown in Figures 5 and 6 and Table 2. When the interface shear stress increases, the load transfer capacity between the fiber and the matrix increases, the initial composite strain remains the same, the initial tangent modulus increases, the transition stress for interface debonding remains the same and the initial fiber broken fraction remains the same.
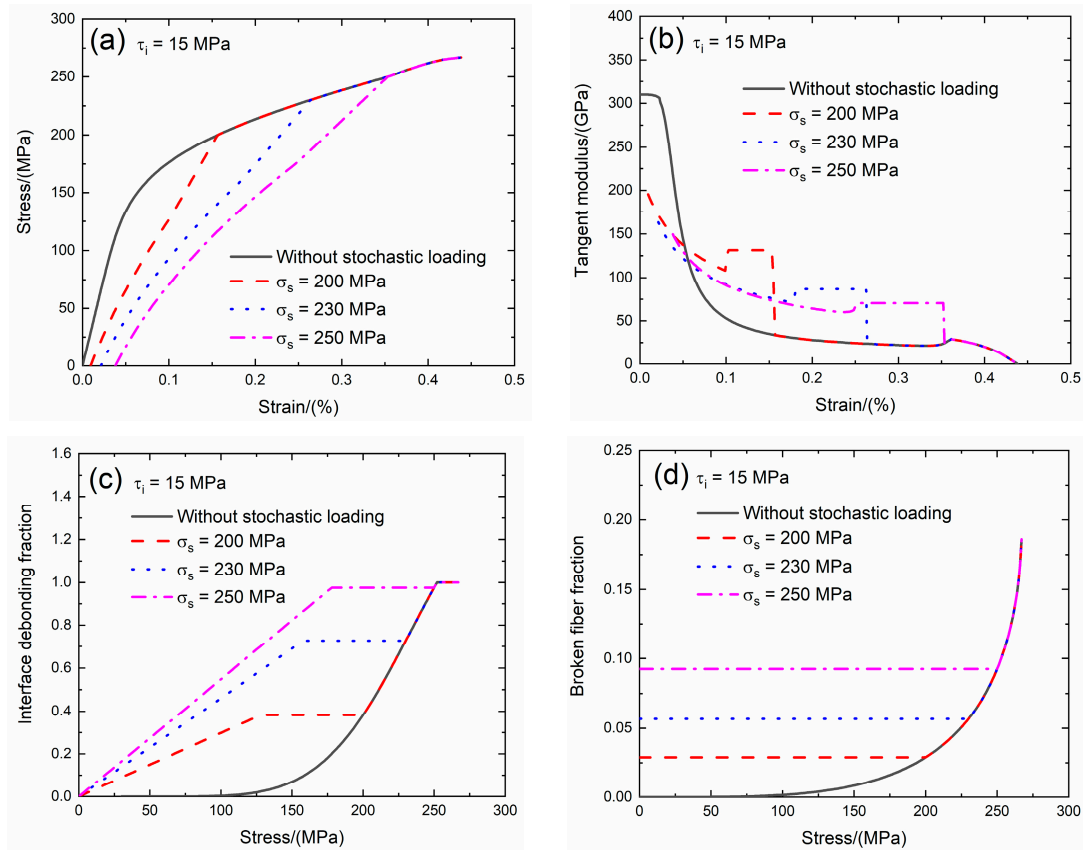
Figure 5. (**a**) The tensile stress–strain curves; (**b**) the tangent modulus versus strain curves; (**c**) the interface debonding fraction versus stress curves; and (**d**) the broken fibers fraction versus stress curves of SiC/SiC composite for conditions without stochastic loading and with stochastic loading of σ_s = 200, 230 and 250 MPa when τ_i = 15 MPa.
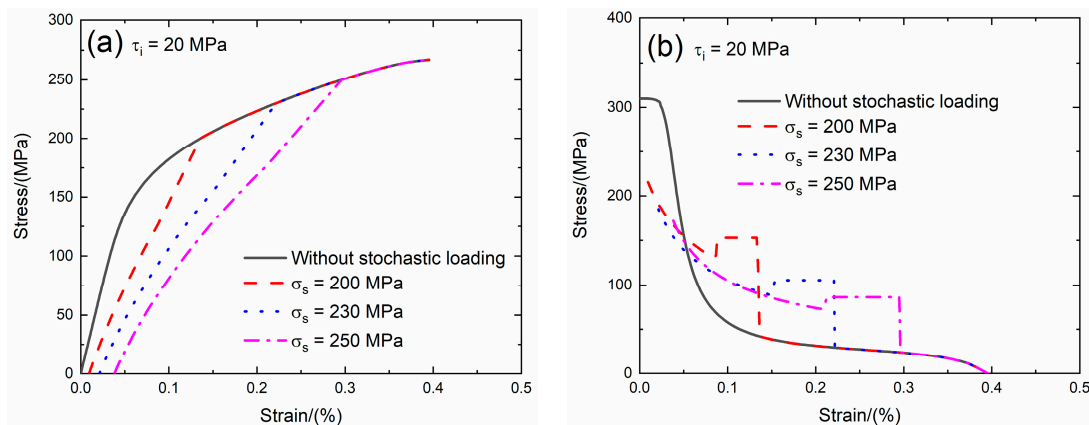
Figure 6. *Cont.*
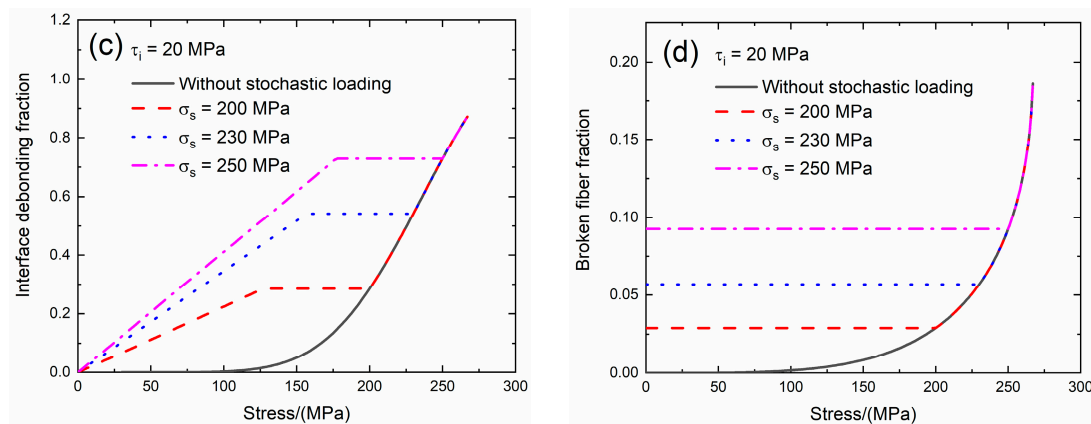
Figure 6. (**a**) The tensile stress–strain curves; (**b**) the tangent modulus versus strain curves; (**c**) the interface debonding fraction versus stress curves; and (**d**) the broken fibers fraction versus stress curves of SiC/SiC composite for conditions without stochastic loading and with stochastic loading of σ_s = 200, 230 and 250 MPa when τ_i = 20 MPa.

Table 2. The effect of interface shear stress (τ_i = 15 and 20 MPa) on tensile stress–strain curve, tangent modulus, interface debonding fraction and broken fiber fraction of SiC/SiC composite subjected to stochastic loading of σ_s = 200, 230 and 250 MPa.

	σ_s = 200 MPa			
	ε_0/(%)	E_p/(GPa)	σ_{tr}/(MPa)	P/(%)
	0.00943	195.6	125.4	0.028
	σ_s = 230 MPa			
τ_i = 15 MPa	ε_0/(%)	E_p/(GPa)	σ_{tr}/(MPa)	P/(%)
	0.021	163	154	0.056
	σ_s = 250 MPa			
	ε_0/(%)	E_p/(GPa)	σ_{tr}/(MPa)	P/(%)
	0.038	149.5	173.8	0.092
	σ_s = 200 MPa			
	ε_0/(%)	E_p/(GPa)	σ_{tr}/(MPa)	P/(%)
	0.00943	215	125.4	0.028
	σ_s = 230 MPa			
τ_i = 20 MPa	ε_0/(%)	E_p/(GPa)	σ_{tr}/(MPa)	P/(%)
	0.021	185	154	0.056
	σ_s = 250 MPa			
	ε_0/(%)	E_p/(GPa)	σ_{tr}/(MPa)	P/(%)
	0.038	171.7	173.8	0.092

When τ_i = 15 MPa under σ_s = 200 MPa, the damages of matrix cracking and interface debonding occur at σ_s = 200 MPa, leading to the increase of the composite initial strain, decreasing of the tangent modulus and increase of the broken fiber fraction. The initial composite strain is ε_0 = 0.00943%; the initial tangent modulus is E_p = 195.6 GPa, the degradation rate of tangent modulus is 37% compared with original specimen and the fiber broken fraction is P = 0.028. With increasing stress to σ_{tr} = 125.4 MPa, the interface debonding fraction increases, the tangent modulus decreases to E_p = 108.1 GPa corresponding to η = 0.374. When the stress increases from σ_{tr} = 125.4 MPa to σ = 200 MPa, the tangent modulus remains constant of E_p = 131.3 GPa with η = 0.382.

Under σ_s = 230 MPa, the initial composite strain is ε_0 = 0.021% due to the damages of matrix cracking and interface debonding at σ_s = 230 MPa; the initial tangent modulus is E_p = 163 GPa, the degradation rate of tangent modulus is 48% compared with original specimen and the fiber broken fraction is P = 0.056. With increasing stress to σ_{tr} = 154 MPa, the interface debonding fraction increases

and the tangent modulus decreases to E_p = 71.5 GPa corresponding to η = 0.727. When the stress increases from σ_{tr} = 154 MPa to σ = 230 MPa, the tangent modulus remains constant of E_p = 86.8 GPa with η = 0.72.

Under σ_s = 250 MPa, the initial composite strain is ε_0 = 0.038% due to the damages of the matrix cracking and interface debonding at σ_s = 250 MPa; the initial tangent modulus is E_p = 149.5 GPa, the degradation rate of the tangent modulus is 52% compared with original specimen and the fiber broken fraction is P = 0.092. With increasing stress to σ_{tr} = 173.8 MPa, the interface debonding fraction increases and the tangent modulus decreases to E_p = 60.7 GPa corresponding to η = 0.952. When the stress increases from σ_{tr} = 173.8 MPa to σ = 250 MPa, the tangent modulus remains constant of E_p = 70.4 GPa with η = 0.975.

When τ_i = 20 MPa under σ_s = 200 MPa, the damages of matrix cracking and interface debonding occur at σ_s = 200 MPa, leading to the increase of the composite initial strain, decreasing of the tangent modulus and increase of the broken fiber fraction. The initial composite strain is ε_0 = 0.00943%; the initial tangent modulus is E_p = 215 GPa, the degradation rate of tangent modulus is 31% compared with original specimen and the fiber broken fraction is P = 0.028. With increasing stress to σ_{tr} = 123.2 MPa, the interface debonding fraction increases and the tangent modulus decreases to E_p = 130 GPa corresponding to η = 0.275. When the stress increases from σ_{tr} = 123.2 MPa to σ = 200 MPa, the tangent modulus remains constant of E_p = 152.9 GPa with η = 0.284.

Under σ_s = 230 MPa, the initial composite strain is ε_0 = 0.021% due to the damages of the matrix cracking and interface debonding at σ_s = 230 MPa; the initial tangent modulus is E_p = 185 GPa, the degradation rate of the tangent modulus is 40% compared with original specimen and the fiber broken fraction is P = 0.056. With increasing stress to σ_{tr} = 154 MPa, the interface debonding fraction increases and the tangent modulus decreases to E_p = 88.6 GPa corresponding to η = 0.53. When the stress increases from σ_{tr} = 154 MPa to σ = 230 MPa, the tangent modulus remains constant of E_p = 105.5 GPa with η = 0.54.

Under σ_s = 250 MPa, the initial composite strain is ε_0 = 0.038% due to the damages of the matrix cracking and interface debonding; the initial tangent modulus is E_p = 171.7 GPa, the degradation rate of tangent modulus is 45% compared with original specimen and the fiber broken fraction is P = 0.092. With increasing stress to σ_{tr} = 173.8 MPa, the interface debonding fraction increases and the tangent modulus decreases to E_p = 72.8 GPa corresponding to η = 0.714. When the stress increases from σ_{tr} = 173.8 MPa to σ = 250 MPa, the tangent modulus remains constant of E_p = 86.3 GPa with η = 0.73.

3.3. Effect of Interface Debonding Energy on Tensile Damage and Fracture of SiC/SiC Composite with Stochastic Loading

The interface debonding energy is a key interface property of CMCs. Domergue et al. [23] estimated the interface debonding energy of unidirectional SiC/CAS composite by analyzing the hysteresis loops and obtained the interface debonding energy is in the range of ζ_d = 0.1 − 0.8 J/m^2. The effect of the interface debonding energy (i.e., ζ_d = 0.1 and 0.3 J/m^2) on the tensile stress–strain curves, tangent modulus, interface debonding fraction and broken fiber fraction of SiC/SiC composite subjected to stochastic loading of σ_s = 180, 220 and 250 MPa are shown in Figures 7 and 8 and Table 3. When the interface debonding energy increases, the initial composite strain, tangent modulus and broken fiber fraction remain the same, the transition stress for interface debonding decreases.
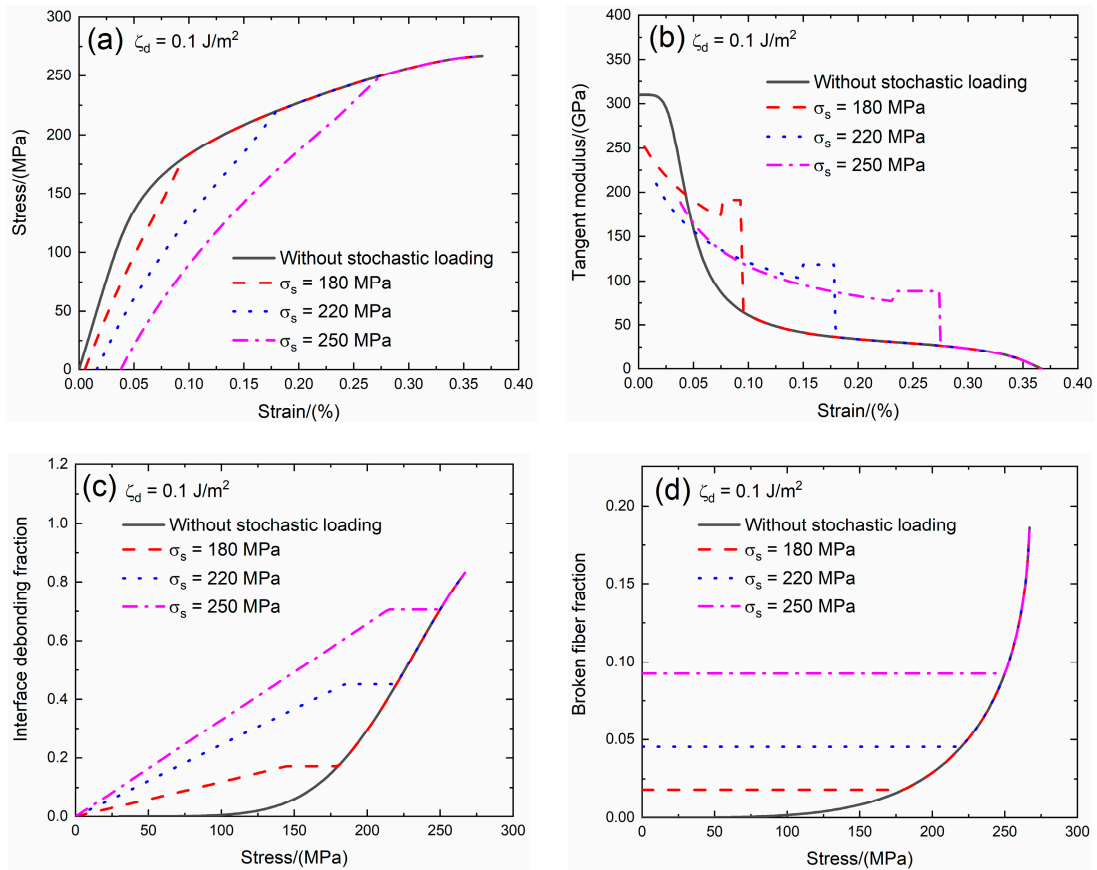
Figure 7. (**a**) The tensile stress–strain curves; (**b**) the tangent modulus versus strain curves; (**c**) the interface debonding fraction versus stress curves; and (**d**) the broken fibers fraction versus stress curves of SiC/SiC composite for conditions without stochastic loading and with stochastic loading of $\sigma_s = 180$, 220 and 250 MPa when $\zeta_d = 0.1$ J/m^2.
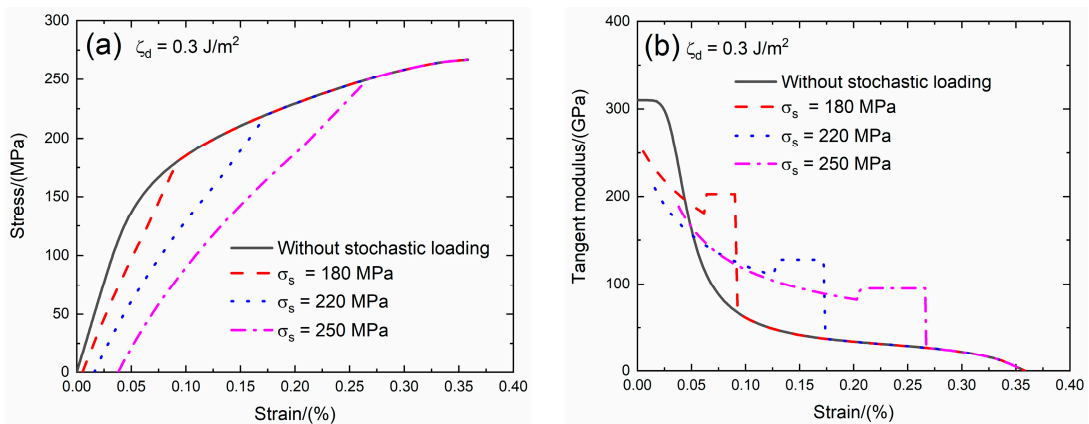
Figure 8. *Cont.*
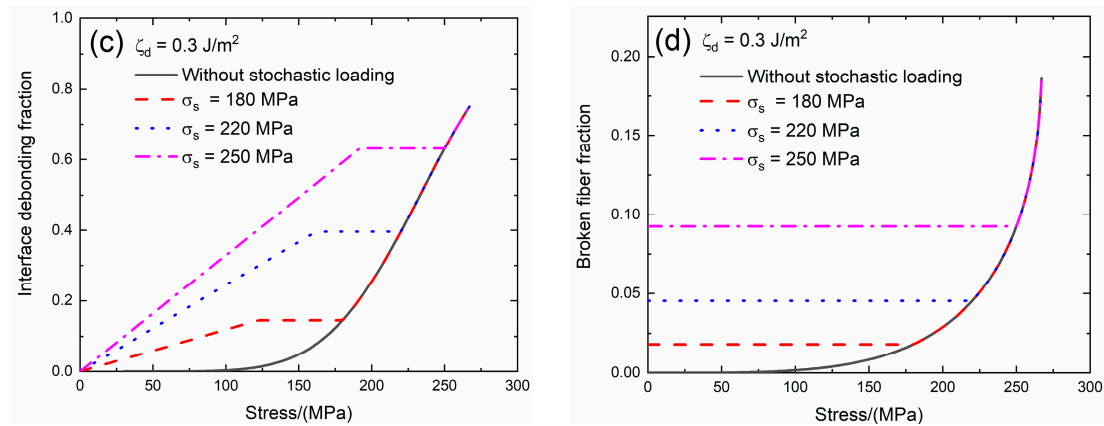
Figure 8. (**a**) The tensile stress–strain curves; (**b**) the tangent modulus versus strain curves; (**c**) the interface debonding fraction versus stress curves; and (**d**) the broken fibers fraction versus stress curves of SiC/SiC composite for conditions without stochastic loading and with stochastic loading of σ_s = 180, 220 and 250 MPa when ζ_d = 0.3 J/m^2.

Table 3. The effect of interface debonding energy (ζ_d = 0.1 and 0.3 J/m^2) on tensile stress–strain curve, tangent modulus, interface debonding fraction and broken fiber fraction of SiC/SiC composite subjected to stochastic loading of σ_s = 180, 220 and 250 MPa.

	σ_s = 180 MPa			
	ε_0/(%)	E_p/(GPa)	σ_{tr}/(MPa)	P/(%)
	0.00537	251.5	140.8	0.018
	σ_s = 220 MPa			
ζ_d = 0.1 J/m^2	ε_0/(%)	E_p/(GPa)	σ_{tr}/(MPa)	P/(%)
	0.0161	209	182.6	0.045
	σ_s = 250 MPa			
	ε_0/(%)	E_p/(GPa)	σ_{tr}/(MPa)	P/(%)
	0.038	188.5	211.2	0.092
	σ_s = 180 MPa			
	ε_0/(%)	E_p/(GPa)	σ_{tr}/(MPa)	P/(%)
	0.00537	251.5	118.8	0.018
	σ_s = 220 MPa			
ζ_d = 0.3 J/m^2	ε_0/(%)	E_p/(GPa)	σ_{tr}/(MPa)	P/(%)
	0.0161	209	158.4	0.045
	σ_s = 250 MPa			
	ε_0/(%)	E_p/(GPa)	σ_{tr}/(MPa)	P/(%)
	0.038	188.5	189.2	0.092

When ζ_d = 0.1 J/m^2 under σ_s = 180 MPa, the damages of matrix cracking and interface debonding occur at σ_s = 180 MPa, leading to the increase of the composite initial strain, decreasing of the tangent modulus and increase of the broken fiber fraction. The initial composite strain is ε_0 = 0.00537%; the initial tangent modulus is E_p = 251.5 GPa, the degradation rate of the tangent modulus is 19% compared with original specimen and the fiber broken fraction is P = 0.018. With increasing stress to σ_{tr} = 140.8 MPa, the interface debonding fraction increases and the tangent modulus decreases to E_p = 171.6 GPa corresponding to η = 0.167. When the stress increases from σ_{tr} = 140.8 MPa to σ = 180 MPa, the tangent modulus remains constant of E_p = 191 GPa with η = 0.171.

Under σ_s = 220 MPa, the initial composite strain is ε_0 = 0.0161% due to the damages of the matrix cracking and interface debonding; the initial tangent modulus is E_p = 209 GPa, the degradation rate of the tangent modulus is 33% compared with original specimen and the fiber broken fraction is P = 0.045. With increasing stress to σ_{tr} = 182.6 MPa, the interface debonding fraction increases and the tangent modulus decreases to E_p = 103.6 GPa corresponding to η = 0.446. When the stress increases from σ_{tr} = 182.6 MPa to σ = 220 MPa, the tangent modulus remains constant of E_p = 118.4 GPa with η = 0.451.

Under σ_s = 250 MPa, the initial composite strain is ε_0 = 0.038% due to the damages of the matrix cracking and interface debonding; the initial tangent modulus is E_p = 188.5 GPa, the degradation rate of the tangent modulus is 40% compared with the original specimen and the fiber broken fraction is P = 0.092. With increasing stress to σ_{tr} = 211.2 MPa, the interface debonding fraction increases and the tangent modulus decreases to E_p = 77 GPa corresponding to η = 0.694. When the stress increases from σ_{tr} = 211.2 MPa to σ = 250 MPa, the tangent modulus remains constant of E_p = 88.2 GPa with η = 0.705.

When ζ_d = 0.3 J/m² under σ_s = 180 MPa, the damages of matrix cracking and interface debonding occur at σ_s = 180 MPa, leading to the increase of the composite initial strain, decreasing of the tangent modulus and increase of the broken fiber fraction. The initial composite strain is ε_0 = 0.00537%; the initial tangent modulus is E_p = 251.5 GPa, the degradation rate of the tangent modulus is 19% compared with the original specimen and the fiber broken fraction is P = 0.018. With increasing stress to σ_{tr} = 118.8 MPa, the interface debonding fraction increases and the tangent modulus decreases to E_p = 180.6 GPa corresponding to η = 0.141. When the stress increases from σ_{tr} = 118.8 MPa to σ = 180 MPa, the tangent modulus remains constant of E_p = 202 GPa with η = 0.144.

Under σ_s = 220 MPa, the initial composite strain is ε_0 = 0.0161%; the initial tangent modulus is E_p = 209 GPa, the degradation rate of tangent modulus is 33% compared with original specimen and the fiber broken fraction is P = 0.045. With increasing stress to σ_{tr} = 158.4 MPa, the interface debonding fraction increases and the tangent modulus decreases to E_p = 110.4 GPa corresponding to η = 0.387. When the stress increases from σ_{tr} = 158.4 MPa to σ = 220 MPa, the tangent modulus remains constant of E_p = 127.6 GPa with η = 0.396.

Under σ_s = 250 MPa, the initial composite strain is ε_0 = 0.038% due to the damages of the matrix cracking and interface debonding; the initial tangent modulus is E_p = 188.5 GPa, the degradation rate of tangent modulus is 40% compared with the original specimen and the fiber broken fraction is P = 0.092. With increasing stress to σ_{tr} = 189.2 MPa, the interface debonding fraction increases and the tangent modulus decreases to E_p = 82 GPa corresponding to η = 0.622. When the stress increases from σ_{tr} = 189.2 MPa to σ = 250 MPa, the tangent modulus remains constant of E_p = 95.1 GPa with η = 0.63.

3.4. Effect of Saturation Matrix Crack Spacing on Tensile Damage and Fracture of SiC/SiC Composite with Stochastic Loading

Li [24] investigated multiple matrix cracking of CMCs with different fiber preforms and found that the saturation matrix cracking spacing is in the range of l_s = 100 and 500 μm. In the present analysis, the effect of the saturation matrix crack spacing (i.e., l_s = 200 and 250 μm) on the tensile stress–strain curves, tangent modulus, interface debonding fraction and broken fiber fraction of SiC/SiC composite subjected to stochastic loading of σ_s = 180, 220 and 250 MPa are shown in Figures 9 and 10 and Table 4. When saturation matrix crack spacing increases, the initial composite strain decreases, the initial tangent modulus increases, the transition stress for interface debonding and initial fiber broken fraction remain the same.
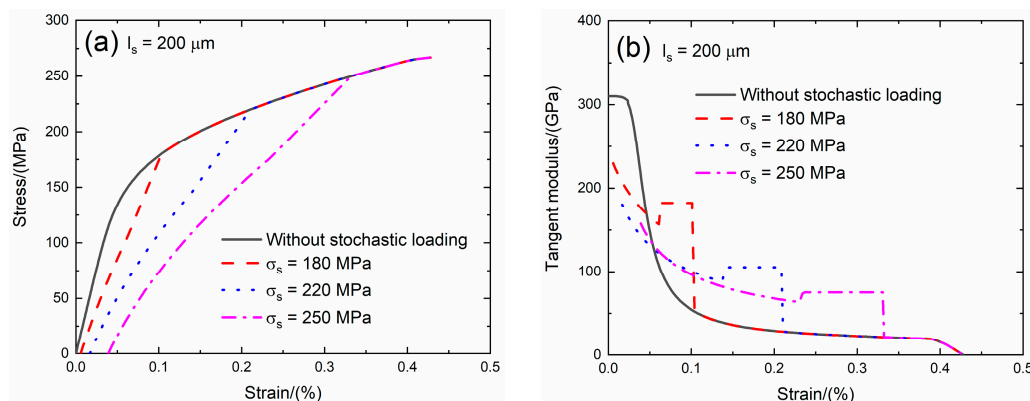
Figure 9. *Cont.*
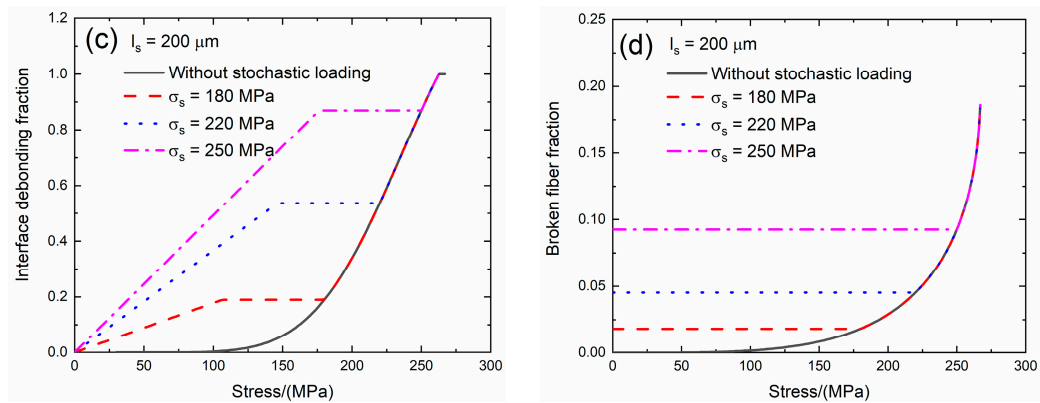
Figure 9. (**a**) The tensile stress–strain curves; (**b**) the tangent modulus versus strain curves; (**c**) the interface debonding fraction versus stress curves; and (**d**) the broken fibers fraction versus stress curves of SiC/SiC composite for conditions without stochastic loading and with stochastic loading of σ_s = 180, 220 and 250 MPa when l_s = 200 μm.
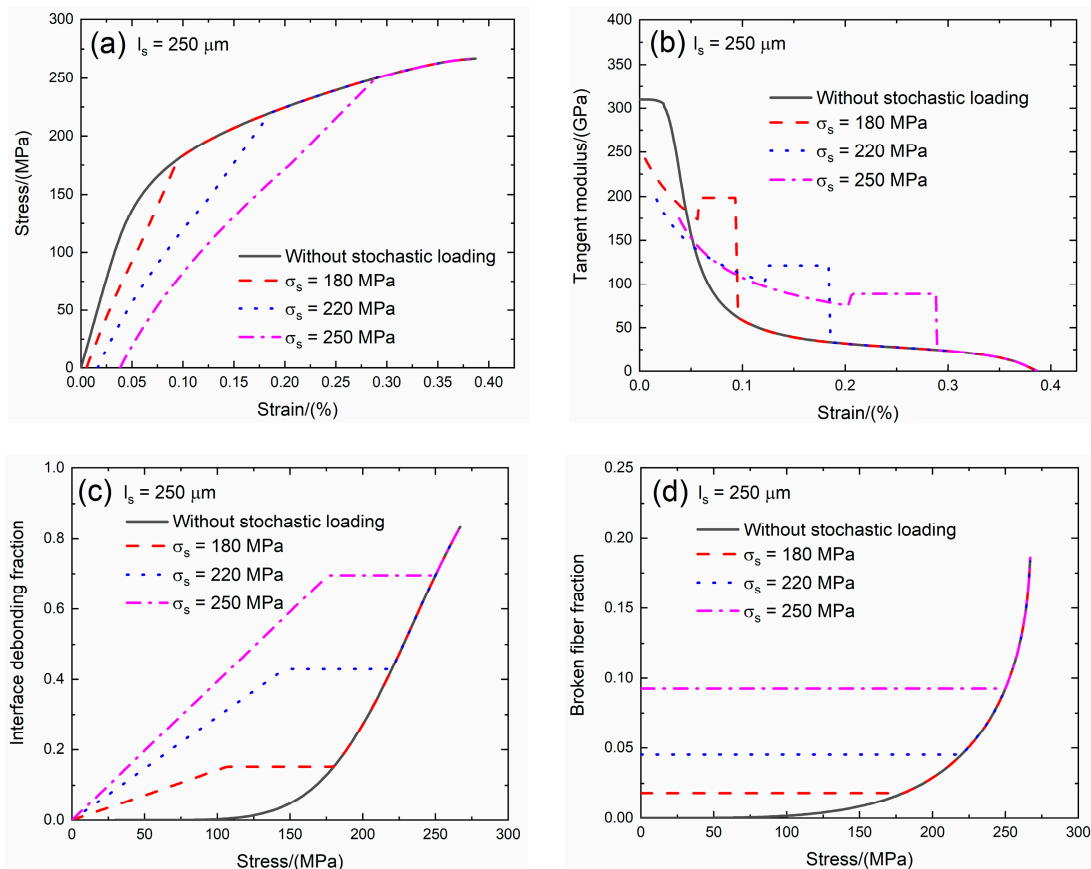
Figure 10. (**a**) The tensile stress–strain curves; (**b**) the tangent modulus versus strain curves; (**c**) the interface debonding fraction versus stress curves; and (**d**) the broken fibers fraction versus stress curves of SiC/SiC composite for conditions without stochastic loading and with stochastic loading of σ_s = 180, 220 and 250 MPa when l_s = 250 μm.

Table 4. The effect of the saturation matrix crack spacing (l_s = 200 and 250 μm) on tensile stress–strain curve, tangent modulus, interface debonding fraction and broken fiber fraction of SiC/SiC composite subjected to stochastic loading of σ_s = 180, 220 and 250 MPa.

		σ_s = 180 MPa		
	ε_0/(%)	E_p/(GPa)	σ_{tr}/(MPa)	P/(%)
	0.00567	229.8	103.4	0.018
		σ_s = 220 MPa		
l_s = 200 μm	ε_0/(%)	E_p/(GPa)	σ_{tr}/(MPa)	P/(%)
	0.0168	180.3	143	0.045
		σ_s = 250 MPa		
	ε_0/(%)	E_p/(GPa)	σ_{tr}/(MPa)	P/(%)
	0.038	157.7	173.8	0.092
		σ_s = 180 MPa		
	ε_0/(%)	E_p/(GPa)	σ_{tr}/(MPa)	P/(%)
	0.00549	242.3	103.4	0.018
		σ_s = 220 MPa		
l_s = 250 μm	ε_0/(%)	E_p/(GPa)	σ_{tr}/(MPa)	P/(%)
	0.0164	196.8	143	0.045
		σ_s = 250 MPa		
	ε_0/(%)	E_p/(GPa)	σ_{tr}/(MPa)	P/(%)
	0.038	174.8	173.8	0.092

When l_s = 200 μm under σ_s = 180 MPa, the damages of matrix cracking and interface debonding occur at σ_s = 200 MPa, leading to the increase of the composite initial strain, decreasing of the tangent modulus and increase of the broken fiber fraction. The initial composite strain is ε_0 = 0.00567% due to the damages of the matrix cracking and interface debonding; the initial tangent modulus is E_p = 229.8 GPa, the degradation rate of tangent modulus is 26% compared with the original specimen and the fiber broken fraction is P = 0.018. With increasing stress to σ_{tr} = 103.4 MPa, the interface debonding fraction increases and the tangent modulus decreases to E_p = 156.5 GPa corresponding to η = 0.184. When the stress increases from σ_{tr} = 103.4 MPa to σ = 180 MPa, the tangent modulus remains constant of E_p = 182.3 GPa with η = 0.189.

Under σ_s = 220 MPa, the initial composite strain is ε_0 = 0.0168% due to the damages of the matrix cracking and the interface debonding; the initial tangent modulus is E_p = 180.3 GPa, the degradation rate of tangent modulus is 42% compared with original specimen and the fiber broken fraction is P = 0.045. With increasing stress to σ_{tr} = 143 MPa, the interface debonding fraction increases and the tangent modulus decreases to E_p = 88.1 GPa corresponding to η = 0.524. When the stress increases from σ_{tr} = 143 MPa to σ = 220 MPa, the tangent modulus remains constant of E_p = 105.2 GPa with η = 0.536.

Under σ_s = 250 MPa, the initial composite strain is ε_0 = 0.038% due to the damages of the matrix cracking and the interface debonding; the initial tangent modulus is E_p = 157.7 GPa, the degradation rate of tangent modulus is 50% compared with original specimen and the fiber broken fraction is P = 0.092. With increasing stress to σ_{tr} = 173.8 MPa, the interface debonding fraction increases and the tangent modulus decreases to E_p = 64 GPa corresponding to η = 0.857. When the stress increases from σ_{tr} = 173.8 MPa to σ = 250 MPa, the tangent modulus remains constant of E_p = 75.3 GPa with η = 0.869.

When l_s = 250 μm under σ_s = 180 MPa, the damages of matrix cracking and interface debonding occur at σ_s = 180 MPa, leading to the increase of the composite initial strain, decreasing of the tangent modulus and increase of the broken fiber fraction. The initial composite strain is ε_0 = 0.00549% due to the damages of the matrix cracking and the interface debonding; the initial tangent modulus is E_p = 242.3 GPa, the degradation rate of tangent modulus is 22% compared with original specimen and the fiber broken fraction is P = 0.018. With increasing stress to σ_{tr} = 103.4 MPa, the interface debonding fraction increases and the tangent modulus decreases to E_p = 173.7 GPa corresponding to η = 0.147.

When the stress increases from σ_{tr} = 103.4.5 MPa to σ = 180 MPa, the tangent modulus remains constant of E_p = 198.7 GPa with η = 0.151.

Under σ_s = 220 MPa, the initial composite strain is ε_0 = 0.0164% due to the damages of the matrix cracking and the interface debonding; the initial tangent modulus is E_p = 196.8 GPa, the degradation rate of tangent modulus is 37% compared with original specimen and the fiber broken fraction is P = 0.045. With increasing stress to σ_{tr} = 143 MPa, the interface debonding fraction increases and the tangent modulus decreases to E_p = 102.8 GPa corresponding to η = 0.42. When the stress increases from σ_{tr} = 143 MPa to σ = 220 MPa, the tangent modulus remains constant of E_p = 121.2 GPa with η = 0.43.

Under σ_s = 250 MPa, the initial composite strain is ε_0 = 0.038% due to the damages of the matrix cracking and the interface debonding; the initial tangent modulus is E_p = 174.8 GPa, the degradation rate of tangent modulus is 44% compared with original specimen and the fiber broken fraction is P = 0.092. With increasing stress to σ_{tr} = 173.8 MPa, the interface debonding fraction increases and the tangent modulus decreases to E_p = 75 GPa corresponding to η = 0.685. When the stress increases from σ_{tr} = 173.8 MPa to σ = 250 MPa, the tangent modulus remains constant of E_p = 88.6 GPa with η = 0.695.

3.5. Effect of Fiber Strength on Tensile Damage and Fracture of SiC/SiC Composite with Stochastic Loading

Guo et al. [25] investigated the SiC fiber strength and found that the SiC fiber strength is in the range between σ_c = 2.3 and 3.7 GPa. In the present analysis, the effect of the fiber strength (i.e., σ_c = 2.0 and 2.5 GPa) on the tensile stress–strain curves, tangent modulus, interface debonding fraction and broken fiber fraction of SiC/SiC composite subjected to stochastic loading of σ_s = 180, 220 and 250 MPa are shown in Figures 11 and 12 and Table 5. When the fiber strength increases, the initial composite strain and fiber broken fraction decrease and the initial tangent composite modulus and transition stress for interface debonding remains the same.
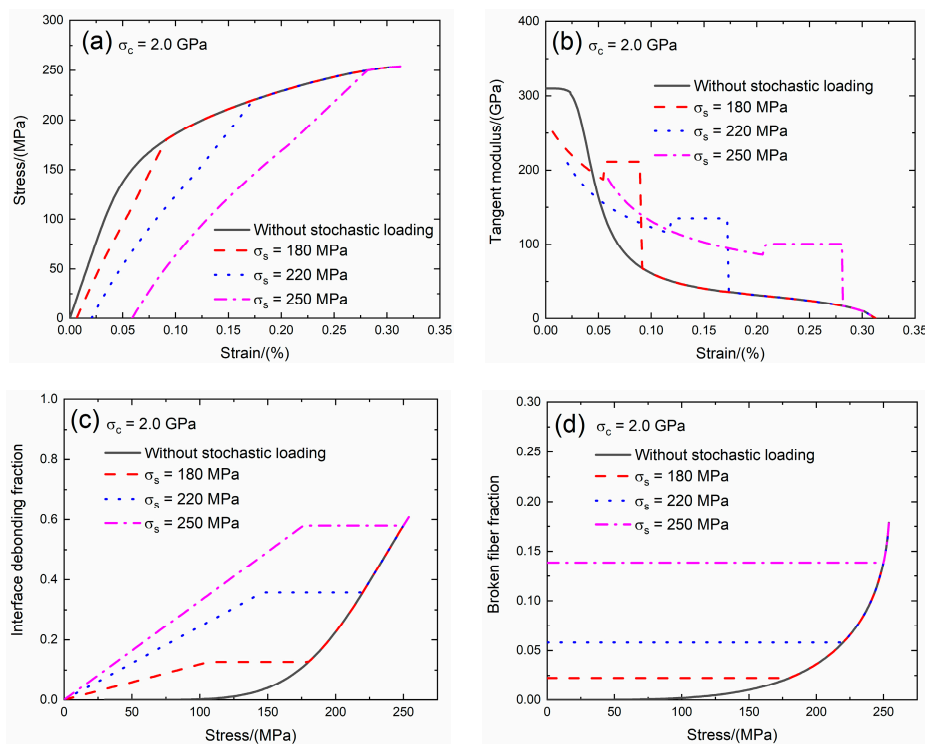
Figure 11. (**a**) The tensile stress–strain curves; (**b**) the tangent modulus versus strain curves; (**c**) the interface debonding fraction versus stress curves; and (**d**) the broken fibers fraction versus stress curves of SiC/SiC composite for conditions without stochastic loading and with stochastic loading of σ_s = 180, 220 and 250 MPa when σ_c = 2.0 GPa.
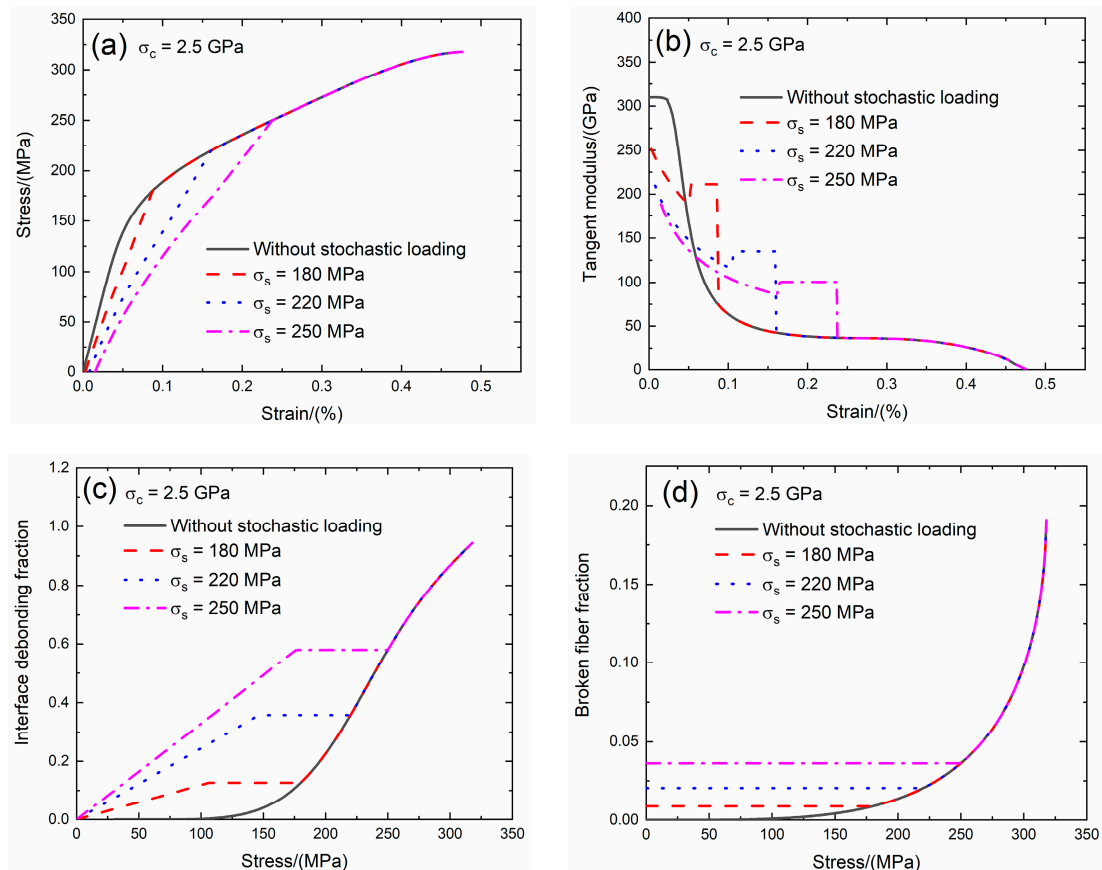
Figure 12. (**a**) The tensile stress–strain curves; (**b**) the tangent modulus versus strain curves; (**c**) the interface debonding fraction versus stress curves; and (**d**) the broken fibers fraction versus stress curves of SiC/SiC composite for conditions without stochastic loading and with stochastic loading of σ_s = 180, 220 and 250 MPa when σ_c = 2.5 GPa.

Table 5. The effect of the fiber strength (σ_c = 2.0 and 2.5 GPa) on tensile stress–strain curve, tangent modulus, interface debonding fraction and broken fiber fraction of SiC/SiC composite subjected to stochastic loading of σ_s = 180, 220 and 250 MPa.

	σ_s = 180 MPa			
	$\varepsilon_0/(\%)$	$E_p/(\text{GPa})$	$\sigma_{tr}/(\text{MPa})$	$P/(\%)$
	0.0065	251.5	103.4	0.022
	σ_s = 220 MPa			
σ_c = 2.0 GPa	$\varepsilon_0/(\%)$	$E_p/(\text{GPa})$	$\sigma_{tr}/(\text{MPa})$	$P/(\%)$
	0.02	209.6	143	0.058
	σ_s = 250 MPa			
	$\varepsilon_0/(\%)$	$E_p/(\text{GPa})$	$\sigma_{tr}/(\text{MPa})$	$P/(\%)$
	0.059	188.5	173.8	0.138
	σ_s = 180 MPa			
	$\varepsilon_0/(\%)$	$E_p/(\text{GPa})$	$\sigma_{tr}/(\text{MPa})$	$P/(\%)$
	0.028	251.5	103.4	0.0087
	σ_s = 220 MPa			
σ_c = 2.5 GPa	$\varepsilon_0/(\%)$	$E_p/(\text{GPa})$	$\sigma_{tr}/(\text{MPa})$	$P/(\%)$
	0.007	209.6	143	0.02
	σ_s = 250 MPa			
	$\varepsilon_0/(\%)$	$E_p/(\text{GPa})$	$\sigma_{tr}/(\text{MPa})$	$P/(\%)$
	0.015	188.5	173.8	0.036

When σ_c = 2.0 GPa under σ_s = 180 MPa, the damages of matrix cracking and interface debonding occur at σ_s = 180 MPa, leading to the increase of the composite initial strain, decreasing of the tangent modulus and increase of the broken fiber fraction. The composite initial strain is ε_0 = 0.0065% due to the damages of the matrix cracking and the interface debonding; the initial tangent modulus is E_p = 251.5 GPa, the degradation rate of tangent modulus is 19% compared with original specimen and the fiber broken fraction is P = 0.022. With increasing stress to σ_{tr} = 103.4 MPa, the interface debonding fraction increases and the tangent modulus decreases to E_p = 187.4 GPa corresponding to η = 0.122. When the stress increases from σ_{tr} = 103.4 MPa to σ = 180 MPa, the tangent modulus remains constant of E_p = 211.3 GPa with η = 0.126.

Under σ_s = 220 MPa, the initial composite strain is ε_0 = 0.02% due to the damages of the matrix cracking and the interface debonding; the initial tangent modulus is E_p = 209.6 GPa, the degradation rate of tangent modulus is 33% compared with original specimen and the fiber broken fraction is P = 0.058. With increasing stress to σ_{tr} = 143 MPa, the interface debonding fraction increases and the tangent modulus decreases to E_p = 115.7 GPa corresponding to η = 0.349. When the stress increases from σ_{tr} = 143 MPa to σ = 220 MPa, the tangent modulus remains constant of E_p = 134.9 GPa with η = 0.357.

Under σ_s = 250 MPa, the initial composite strain is ε_0 = 0.059%; the initial tangent modulus is E_p = 188.5 GPa, the degradation rate of tangent modulus is 40% compared with original specimen and the fiber broken fraction is P = 0.138. With increasing stress to σ_{tr} = 173.8 MPa, the interface debonding fraction increases and the tangent modulus decreases to E_p = 86 GPa corresponding to η = 0.571. When the stress increases from σ_{tr} = 173.8 MPa to σ = 250 MPa, the tangent modulus remains constant of E_p = 100.6 GPa with η = 0.579.

When σ_c = 2.5 GPa under σ_s = 180 MPa, the damages of matrix cracking and interface debonding occur at σ_s = 180 MPa, leading to the increase of the composite initial strain, decreasing of the tangent modulus and increase of the broken fiber fraction. The initial composite strain is ε_0 = 0.0028% due to the damages of the matrix cracking and the interface debonding; the initial tangent modulus is E_p = 251.5 GPa, the degradation rate of tangent modulus is 19% compared with original specimen and the fiber broken fraction is P = 0.0087. With increasing stress to σ_{tr} = 103.4 MPa, the interface debonding fraction increases and the tangent modulus decreases to E_p = 187.4 GPa corresponding to η = 0.122. When the stress increases from σ_{tr} = 103.4 MPa to σ = 180 MPa, the tangent modulus remains constant of E_p = 211.3 GPa with η = 0.126.

Under σ_s = 220 MPa, the initial composite strain is ε_0 = 0.007% due to the damages of the matrix cracking and the interface debonding; the initial tangent modulus is E_p = 209.6 GPa, the degradation rate of tangent modulus is 33% compared with original specimen and the fiber broken fraction is P = 0.02. With increasing stress to σ_{tr} = 143 MPa, the interface debonding fraction increases and the tangent modulus decreases to E_p = 115.7 GPa corresponding to η = 0.344. When the stress increases from σ_{tr} = 140.8 MPa to σ = 220 MPa, the tangent modulus remains constant of E_p = 134.9 GPa with η = 0.357.

Under σ_s = 250 MPa, the initial composite strain is ε_0 = 0.015%; the initial tangent modulus is E_p = 188.5 GPa, the degradation rate of the tangent modulus is 40% compared with original specimen and the fiber broken fraction is P = 0.036. With increasing stress to σ_{tr} = 173.8 MPa, the interface debonding fraction increases and the tangent modulus decreases to E_p = 86 GPa corresponding to η = 0.571. When the stress increases from σ_{tr} = 173.8 MPa to σ = 250 MPa, the tangent modulus remains constant of E_p = 100.6 GPa with η = 0.579.

4. Experimental Comparisons

Li et al. [4], Liu [5], Guo and Kagawa [6] and Morscher [7] investigated tensile behavior of unidirectional and 2D SiC/SiC composites at room temperature. In this section, using the developed damage models and micromechanical constitutive models for the conditions of matrix cracking, interface debonding and fiber failure, the experimental tensile stress–strain curves are predicted.

The comparisons between tensile stress–strain curves with and without stochastic loading are analyzed. The relationships between the stochastic loading stress levels, tangent modulus, interface debonding fraction and fiber broken fraction are established.

4.1. 2D SiC/SiC under Stochastic Loading of 140, 180, 200 and 240 MPa

Li et al. [4] investigated the tensile behavior of 2D SiC/SiC composite at room temperature. The composite was fabricated using chemical vapor infiltration (CVI) method. The tensile test was performed under displacement control with the speed of 0.3 mm/min. The experimental tensile stress–strain curves, tangent modulus versus strain curves, interface debonding fraction and broken fiber fraction versus stress curves of 2D SiC/SiC composite without stochastic loading and with stochastic loading at σ_s = 140, 180, 200 and 240 MPa at room temperature are shown in Figure 13 and Table 6. When stochastic loading stress increases, the initial composite strain increases, the initial tangent modulus decreases, the transition stress for interface debonding increases and the initial fiber broken fraction increases.
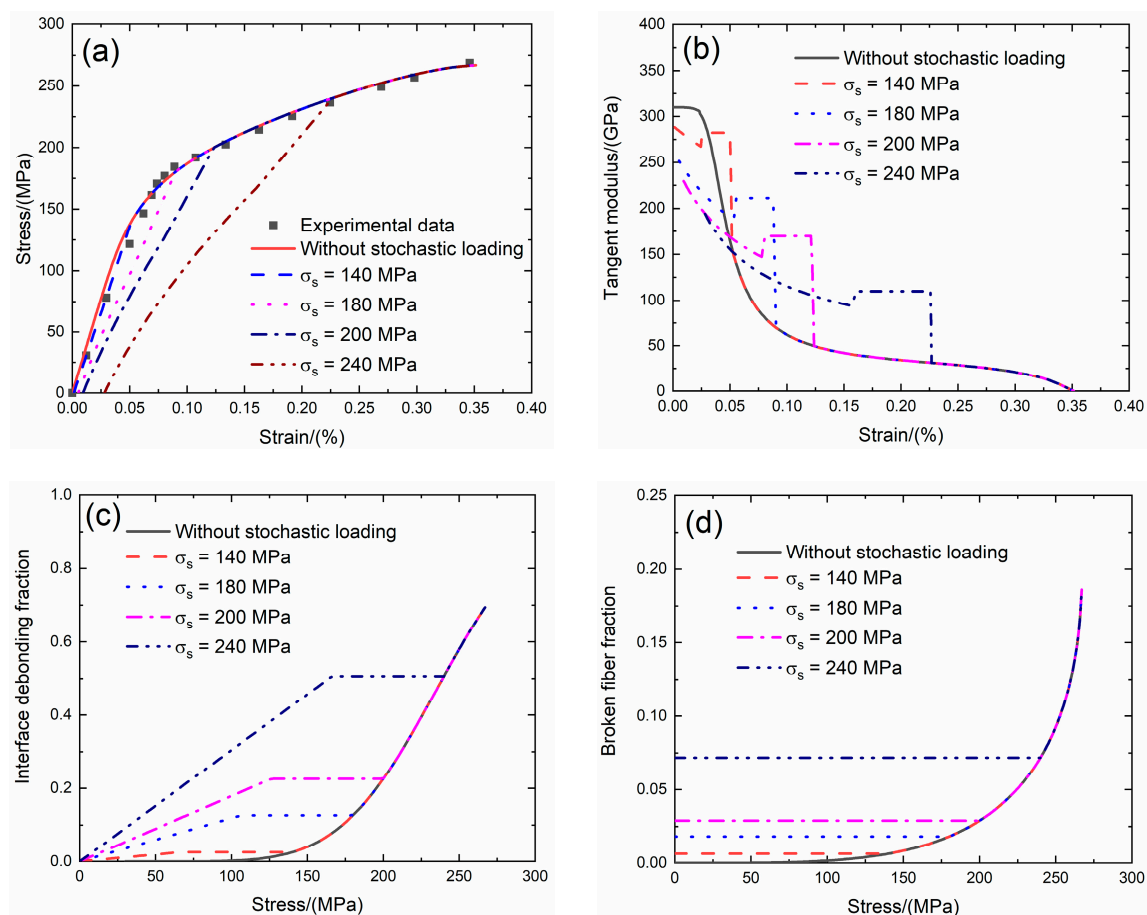
Figure 13. (**a**) The tensile stress–strain curves; (**b**) the tangent modulus versus strain curves; (**c**) the interface debonding fraction versus stress curves; and (**d**) the broken fibers fraction versus stress curves of 2D SiC/SiC composite for conditions without stochastic loading and with stochastic loading of σ_s = 140, 180, 200 and 240 MPa.

Table 6. The tensile stress–strain curve, tangent modulus, interface debonding fraction and broken fiber fraction of 2D SiC/SiC composite subjected to stochastic loading of σ_s = 140, 180, 200 and 240 MPa.

ε_0/(%)	E_p/(GPa)	σ_{tr}/(MPa)	P
σ_s = 140 MPa.			
0.001	288	63.8	0.006
σ_s = 180 MPa			
0.005	251	103.4	0.018
σ_s = 180 MPa			
0.009	229.5	123.2	0.028
σ_s = 180 MPa			
0.028	194.2	162.8	0.078

Under σ_s = 140 MPa, the initial strain is ε_0 = 0.001%; the initial tangent modulus is E_p = 288 GPa, the degradation rate of tangent modulus is 7% compared with original specimen and the fiber broken fraction is P = 0.006. With increasing stress to σ_{tr} = 63.8 MPa, the tangent modulus decreases to E_p = 267.4 GPa corresponding to η = 0.024. When the stress increases from σ_{tr} = 63.8 MPa to σ = 140 MPa, the tangent modulus remains constant of E_p = 282.3 GPa with η = 0.025.

Under σ_s = 180 MPa, the initial strain is ε_0 = 0.005%; the initial tangent modulus is E_p = 251 GPa, the degradation rate of tangent modulus is 19% compared with original specimen and the fiber broken fraction is P = 0.018. With increasing stress to σ_{tr} = 103.4 MPa, the tangent modulus decreases to E_p = 187.4 GPa corresponding to η = 0.122. When the stress increases from σ_{tr} = 103.4 MPa to σ = 180 MPa, the tangent modulus remains constant of E_p = 211.3 GPa with η = 0.126.

Under σ_s = 200 MPa, the initial strain is ε_0 = 0.009%; the initial tangent modulus is E_p = 229.5 GPa, the degradation rate of tangent modulus is 26% compared with original specimen and the fiber broken fraction is P = 0.028. With increasing stress to σ_{tr} = 123.2 MPa, the tangent modulus decreases to E_p = 147.1 GPa corresponding to η = 0.22. When the stress increases from σ_{tr} = 123.2 MPa to σ = 200 MPa, the tangent modulus remains constant of E_p = 169.7 GPa with η = 0.226.

Under σ_s = 240 MPa, the initial strain is ε_0 = 0.028%; the initial tangent modulus is E_p = 194.2 GPa, the degradation rate of tangent modulus is 38% compared with original specimen and the fiber broken fraction is P = 0.078. With increasing stress to σ_{tr} = 162.8 MPa, the tangent modulus decreases to E_p = 94 GPa corresponding to η = 0.49. When the stress increases from σ_{tr} = 162.8 MPa to σ = 240 MPa, the tangent modulus remains constant of E_p = 109.8 GPa with η = 0.5.

4.2. UD and 2D SiC/SiC under Stochastic Loading

Liu [5] investigated the tensile behavior of unidirectional and 2D SiC/SiC composites at room temperature. The tensile test was performed under displacement control with the loading rate of 0.2 mm/min.

For unidirectional SiC/SiC composite, the tensile stress–strain curves, tangent modulus versus strain curves, interface debonding fraction and broken fiber fraction versus stress curves without stochastic loading and with stochastic loading at σ_s = 140, 180, 200 and 220 MPa at room temperature are shown in Figure 14 and Table 7.
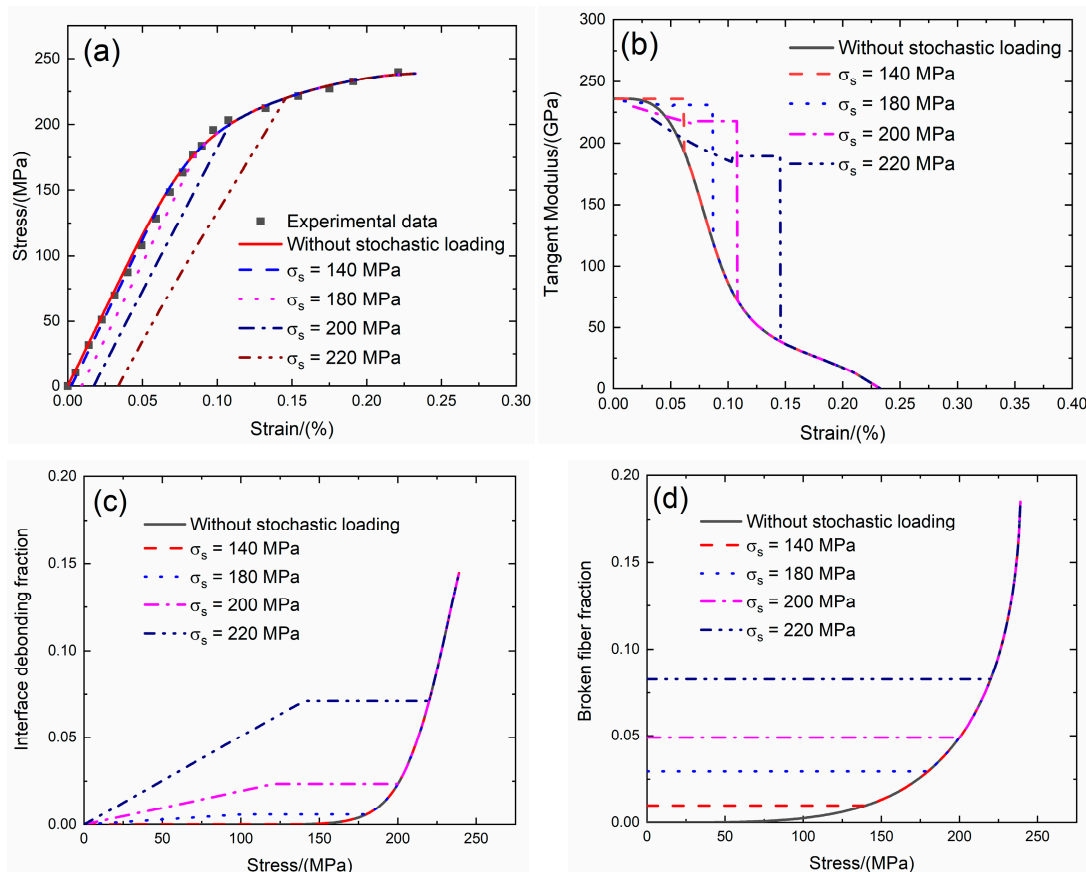
Figure 14. (**a**) The tensile stress–strain curves; (**b**) the tangent modulus versus strain curves; (**c**) the interface debonding fraction versus stress curves; and (**d**) the broken fibers fraction versus stress curves of UD SiC/SiC composite for conditions without stochastic loading and with stochastic loading of σ_s = 140, 180, 200 and 220 MPa.

Table 7. The tensile stress–strain curve, tangent modulus, interface debonding fraction and broken fiber fraction of unidirectional SiC/SiC composite subjected to stochastic loading of σ_s = 140, 180, 200 and 220 MPa.

σ_s = 140 MPa			
ε_0/(%)	E_p/(GPa)	σ_{tr}/(MPa)	P
0.002	235.9	58.8	0.01
σ_s = 180 MPa			
ε_0/(%)	E_p/(GPa)	σ_{tr}/(MPa)	P
0.009	234	98.4	0.03
σ_s = 200 MPa			
ε_0/(%)	E_p/(GPa)	σ_{tr}/(MPa)	P
0.017	229.6	118.8	0.048
σ_s = 220 MPa			
ε_0/(%)	E_p/(GPa)	σ_{tr}/(MPa)	P
0.033	220.1	139	0.082

Under σ_s = 140 MPa, the initial strain is ε_0 = 0.002%; the initial tangent modulus is E_p = 235.9 GPa, the degradation rate of tangent modulus is 1% compared with original specimen and the fiber broken fraction is P = 0.01. With increasing stress to σ_{tr} = 58.8 MPa, the tangent modulus decreases to

E_p = 235.7 GPa corresponding to η = 0.0001. When the stress increases from σ_{tr} = 58.8 MPa to σ = 140 MPa, the tangent modulus remains constant of E_p = 235.8 GPa with η = 0.0001.

Under σ_s = 180 MPa, the initial strain is ε_0 = 0.009%; the initial tangent modulus is E_p = 234 GPa, the degradation rate of tangent modulus is 1.1% compared with original specimen and the fiber broken fraction is P = 0.03. With increasing stress to σ_{tr} = 98.4 MPa, the tangent modulus decreases to E_p = 230.1 GPa corresponding to η = 0.005. When the stress increases from σ_{tr} = 98.4 MPa to σ = 180 MPa, the tangent modulus remains constant of E_p = 230.9 GPa with η = 0.005.

Under σ_s = 200 MPa, the initial strain is ε_0 = 0.0174%; the initial tangent modulus is E_p = 229.6 GPa, the degradation rate of tangent modulus is 2.8% compared with original specimen and the fiber broken fraction is P = 0.048. With increasing stress to σ_{tr} = 118.8 MPa, the tangent modulus decreases to E_p = 215.4 GPa corresponding to η = 0.023. When the stress increases from σ_{tr} = 118.8 MPa to σ = 200 MPa, the tangent modulus remains constant of E_p = 217.8 GPa with η = 0.023.

Under σ_s = 220 MPa, the initial strain is ε_0 = 0.033%; the initial tangent modulus is E_p = 220.1 GPa, the degradation rate of tangent modulus is 6.8% compared with original specimen and the fiber broken fraction is P = 0.082. With increasing stress to σ_{tr} = 139 MPa, the tangent modulus decreases to E_p = 184.5 GPa corresponding to η = 0.07. When the stress increases from σ_{tr} = 139 MPa to σ = 220 MPa, the tangent modulus remains constant of E_p = 189.2 GPa with η = 0.071.

For 2D SiC/SiC composite, the tensile stress–strain curves, tangent modulus versus strain curves, interface debonding fraction and broken fiber fraction versus stress curves without stochastic loading and with stochastic loading at σ_s = 80, 100 and 120 MPa at room temperature are shown in Figure 15 and Table 8.
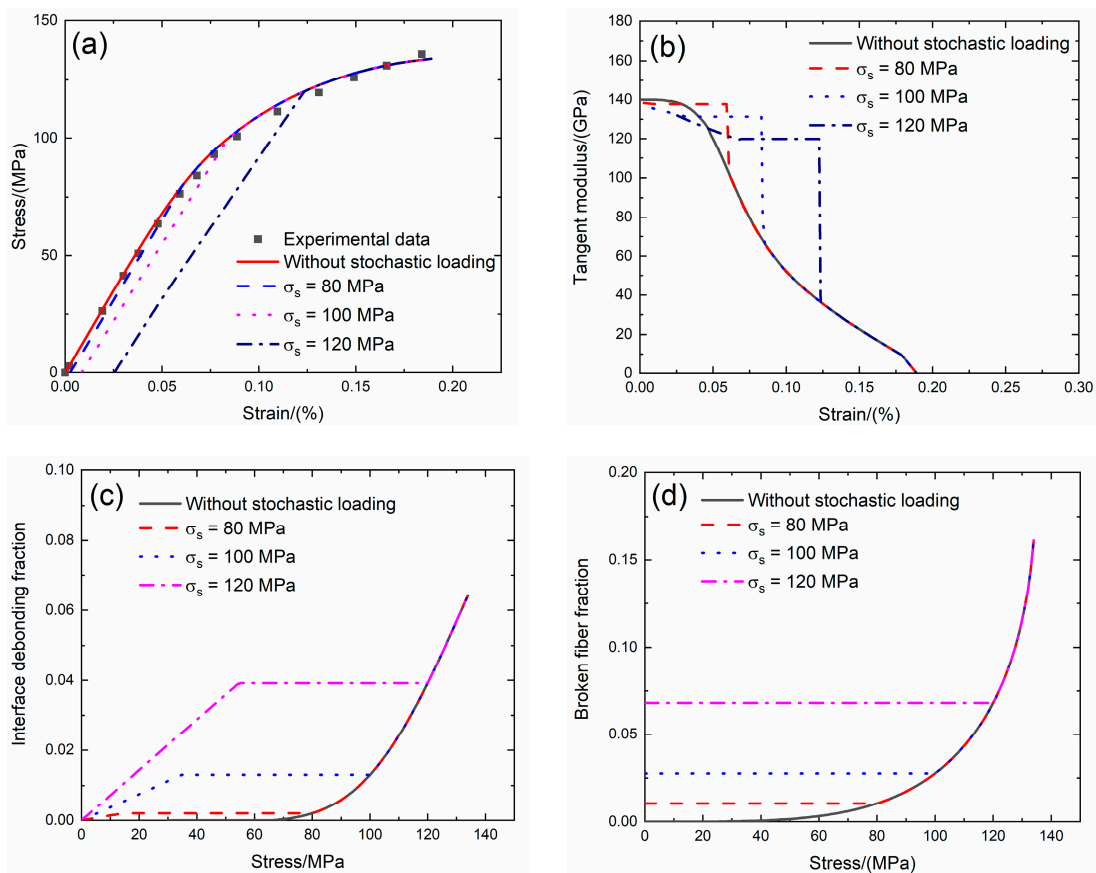
Figure 15. (**a**) The tensile stress–strain curves; (**b**) the tangent modulus versus strain curves; (**c**) the interface debonding fraction versus stress curves; and (**d**) the broken fibers fraction versus stress curves of 2D SiC/SiC composite for conditions without stochastic loading and with stochastic loading of σ_s = 80, 100 and 120 MPa.

Table 8. The tensile stress–strain curve, tangent modulus, interface debonding fraction and broken fiber fraction of 2D SiC/SiC composite subjected to stochastic loading of σ_s = 80, 100 and 120 MPa.

σ_s = 80 MPa			
ε_0/(%)	E_p/(GPa)	σ_{tr}/(MPa)	P
0.002	138.3	13.2	0.01
σ_s = 100 MPa			
ε_0/(%)	E_p/(GPa)	σ_{tr}/(MPa)	P
0.008	135.6	32.4	0.027
σ_s = 120 MPa			
ε_0/(%)	E_p/(GPa)	σ_{tr}/(MPa)	P
0.025	131.9	52.8	0.068

Under σ_s = 80 MPa, the initial strain is ε_0 = 0.002%; the initial tangent modulus is E_p = 138.3 GPa, the degradation rate of tangent modulus is 1.2% compared with original specimen and the fiber broken fraction is P = 0.01. With increasing stress to σ_{tr} = 13.2 MPa, the tangent modulus decreases to E_p = 137.6 GPa corresponding to η = 0.001. When stress increases from σ_{tr} = 13.2 MPa to σ = 80 MPa, the tangent modulus remains constant of E_p = 137.7 GPa with η = 0.002.

Under σ_s = 100 MPa, the initial strain is ε_0 = 0.008%; the initial tangent modulus is E_p = 135.6 GPa, the degradation rate of tangent modulus is 3.1% compared with original specimen and the fiber broken fraction is P = 0.027. With increasing stress to σ_{tr} = 32.4 MPa, the tangent modulus decreases to E_p = 131 GPa corresponding to η = 0.012. When stress increases from σ_{tr} = 32.4 MPa to σ = 100 MPa, the tangent modulus remains constant of E_p = 131.3 GPa with η = 0.013.

Under σ_s = 120 MPa, the initial strain is ε_0 = 0.025%; the initial tangent modulus is E_p = 131.9 GPa, the degradation rate of tangent modulus is 5.8% compared with original specimen and the fiber broken fraction is P = 0.068. With increasing stress to σ_{tr} = 52.8 MPa, the tangent modulus decreases to E_p = 119.5 GPa corresponding to η = 0.038. When stress increases from σ_{tr} = 52.8 MPa to σ = 120 MPa, the tangent modulus remains constant of E_p = 119.5 GPa with η = 0.039.

4.3. 2D SiC/SiC under Stochastic Loading of 80, 100 and 120 MPa

Guo and Kagawa [6] investigated the tensile behavior of 2D plain-woven fabric SiC/SiC composite fabricated by the PIP process. The quasi-static tensile test was conducted under displacement control with the rate of 0.5 mm/min. The tensile stress–strain curves, tangent modulus versus strain curves, interface debonding fraction and broken fiber fraction versus stress curves without stochastic loading and with stochastic loading at σ_s = 80, 100 and 120 MPa at room temperature are shown in Figure 16 and Table 9.
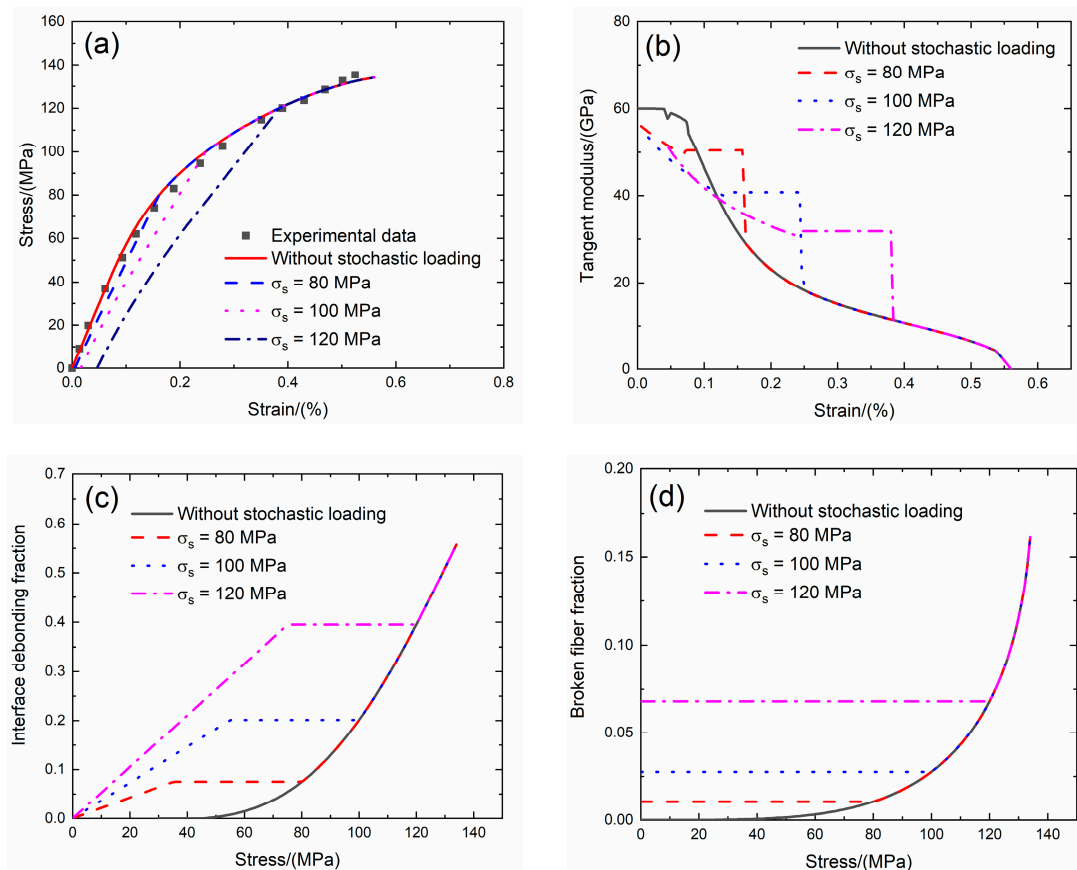
Figure 16. (**a**) The tensile stress–strain curves; (**b**) the tangent modulus versus strain curves; (**c**) the interface debonding fraction versus stress curves; and (**d**) the broken fibers fraction versus stress curves of 2D SiC/SiC composite for conditions without stochastic loading and with stochastic loading of σ_s = 80, 100 and 120 MPa.

Table 9. The tensile stress–strain curve, tangent modulus, interface debonding fraction and broken fiber fraction of 2D SiC/SiC composite subjected to stochastic loading of σ_s = 80, 100 and 120 MPa.

σ_s = 80 MPa			
ε_0/(%)	E_p/(GPa)	σ_{tr}/(MPa)	P
0.005	56	33.6	0.01
σ_s = 100 MPa			
ε_0/(%)	E_p/(GPa)	σ_{tr}/(MPa)	P
0.016	53.5	52.8	0.027
σ_s = 120 MPa			
ε_0/(%)	E_p/(GPa)	σ_{tr}/(MPa)	P
0.046	51	73.2	0.068

Under σ_s = 80 MPa, the initial strain is ε_0 = 0.005%; the initial tangent modulus is E_p = 56 GPa, the degradation rate of tangent modulus is 6.7% compared with original specimen and the fiber broken fraction is P = 0.01. With increasing stress to σ_{tr} = 33.6 MPa, the tangent modulus decreases to E_p = 49.4 GPa corresponding to η = 0.07. When stress increases from σ_{tr} = 33.6 MPa to σ = 80 MPa, the tangent modulus remains constant of E_p = 50.4 GPa with η = 0.074.

Under σ_s = 100 MPa, the initial strain is ε_0 = 0.016%; the initial tangent modulus is E_p = 53.5 GPa, the degradation rate of tangent modulus is 11% compared with original specimen and the fiber broken fraction is P = 0.027. With increasing stress to σ_{tr} = 52.8 MPa, the tangent modulus decreases to

E_p = 39.7 GPa corresponding to η = 0.19. When stress increases from σ_{tr} = 52.8 MPa to σ = 100 MPa, the tangent modulus remains constant of E_p = 40.7 GPa with η = 0.2.

Under σ_s = 120 MPa, the initial strain is ε_0 = 0.046%; the initial tangent modulus is E_p = 51 GPa, the degradation rate of tangent modulus is 15% compared with original specimen and the fiber broken fraction is P = 0.068. With increasing stress to σ_{tr} = 73.2 MPa, the tangent modulus decreases to E_p = 30.8 GPa corresponding to η = 0.39. When stress increases from σ_{tr} = 73.2 MPa to σ = 120 MPa, the tangent modulus remains constant of E_p = 31.7 GPa with η = 0.395.

4.4. 2D SiC/SiC under Stochastic Loading of 180, 220, 260 and 300 MPa

Morscher [7] investigated the tensile behavior of 2D SiC/SiC composite at room temperature. The tensile test was conducted under load control. The tensile stress–strain curves, tangent modulus versus strain curves, interface debonding fraction and broken fiber fraction versus stress curves without stochastic loading and with stochastic loading at σ_s = 180, 220, 260 and 300 MPa are shown in Figure 17 and Table 10.
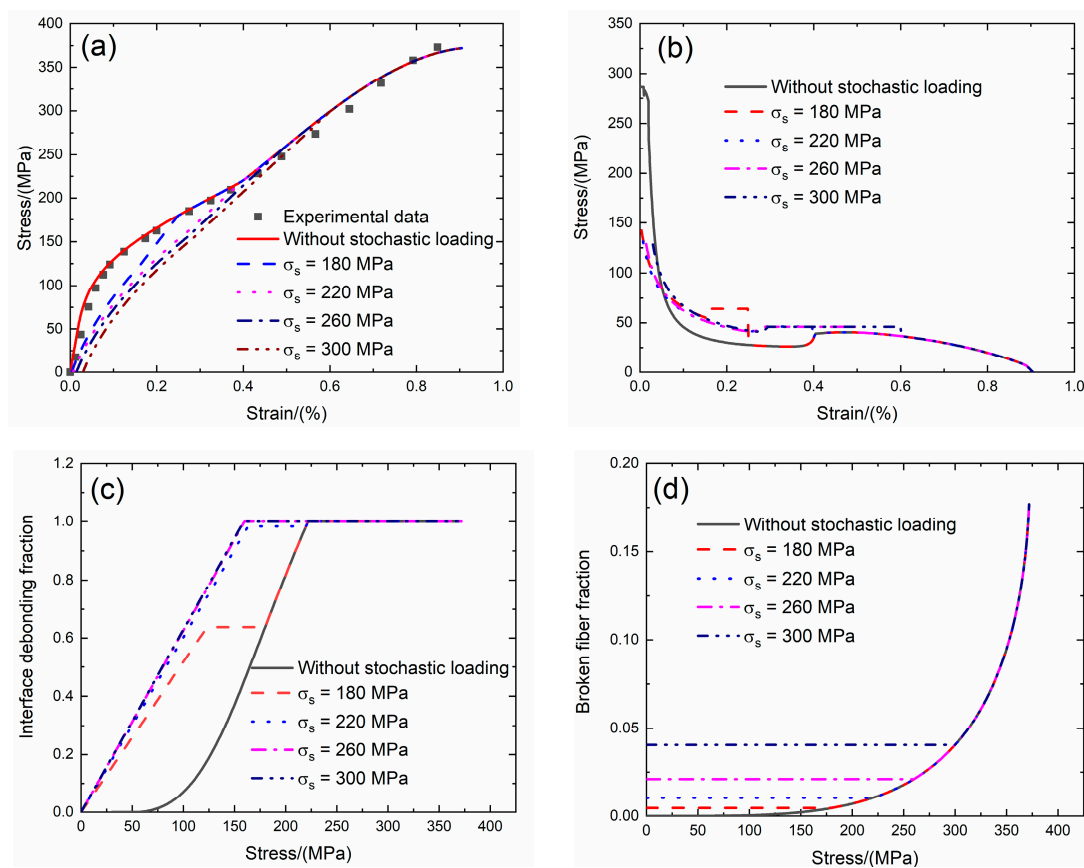
Figure 17. (**a**) The tensile stress–strain curves; (**b**) the tangent modulus versus strain curves; (**c**) the interface debonding fraction versus stress curves; and (**d**) the broken fibers fraction versus stress curves of 2D SiC/SiC composite for conditions without stochastic loading and with stochastic loading of σ_s = 180, 220, 260 and 300 MPa.

Table 10. The tensile stress–strain curve, tangent modulus, interface debonding fraction and broken fiber fraction of 2D SiC/SiC composite subjected to stochastic loading of σ_s = 180, 220, 260 and 300 MPa.

$\varepsilon_0/(\%)$	$E_p/(\text{GPa})$	$\sigma_{tr}/(\text{MPa})$	P
σ_s = 180 MPa			
0.003	142.3	122	0.004
σ_s = 220 MPa			
0.007	131.4	162	0.01
σ_s = 260 MPa			
0.014	128.7	150	0.021
σ_s = 300 MPa			
0.029	128.3	148	0.04

Under σ_s = 180 MPa, the initial strain is ε_0 = 0.003%; the initial tangent modulus is E_p = 142.3 GPa, the degradation rate of tangent modulus is 50% compared with original specimen and the fiber broken fraction is P = 0.004. With increasing stress to σ_{tr} = 122 MPa, the tangent modulus decreases to E_p = 53.9 GPa corresponding to η = 0.63. When stress increases from σ_{tr} = 122 MPa to σ = 180 MPa, the tangent modulus remains constant of E_p = 63.9 GPa with η = 0.638.

Under σ_s = 220 MPa, the initial strain is ε_0 = 0.007%; the initial tangent modulus is E_p = 131.4 GPa, the degradation rate of tangent modulus is 54% compared with original specimen and the fiber broken fraction is P = 0.01. With increasing stress to σ_{tr} = 162 MPa, the tangent modulus decreases to E_p = 42 GPa corresponding to η = 0.63. When stress increases from σ_{tr} = 122 MPa to σ = 180 MPa, the tangent modulus remains constant of E_p = 63.9 GPa with η = 0.97.

Under σ_s = 260 MPa, the initial strain is ε_0 = 0.014%; the initial tangent modulus is E_p = 128.7 GPa, the degradation rate of tangent modulus is 55% compared with original specimen and the fiber broken fraction is P = 0.021. With increasing stress to σ_{tr} = 150 MPa, the tangent modulus decreases to E_p = 41.3 GPa corresponding to η = 0.93. When stress increases from σ_{tr} = 150 MPa to σ = 260 MPa, the tangent modulus remains constant of E_p = 46 GPa with η = 1.0.

Under σ_s = 300 MPa, the initial strain is ε_0 = 0.029%; the initial tangent modulus is E_p = 128.3 GPa, the degradation rate of tangent modulus is 55.1% compared with original specimen and the fiber broken fraction is P = 0.04. With increasing stress to σ_{tr} = 148 MPa, the tangent modulus decreases to E_p = 41.3 GPa corresponding to η = 0.93. When stress increases from σ_{tr} = 148 MPa to σ = 300 MPa, the tangent modulus remains constant of E_p = 46 GPa with η = 1.0.

5. Conclusions

In this paper, the effect of stochastic loading on tensile damage and fracture of fiber-reinforced CMCs is investigated. A micromechanical constitutive model is developed considering multiple damage mechanisms under tensile loading. The relationship between stochastic stress, tangent modulus, interface debonding and fiber broken is established. The effects of fiber volume, interface shear stress, interface debonding energy, saturation matrix crack spacing and fiber strength on tensile stress–strain curve, tangent modulus, interface debonding fraction and fiber broken fraction are analyzed. The experimental tensile damage and fracture of unidirectional and 2D SiC/SiC composites subjected to different stochastic loading stress are predicted.

(1)   When fiber volume increases, the initial composite strain decreases, the initial tangent modulus increases, the transition stress for interface debonding decreases and the initial fiber broken fraction decreases;

(2)   When the interface shear stress increases, the initial composite strain remains the same, the initial tangent modulus increases, the transition stress for interface debonding remains the same and the initial fiber broken fraction remains the same;

(3)   When the interface debonding energy increases, the initial composite strain, tangent modulus and broken fiber fraction remain the same and the transition stress for interface debonding decreases;

(4)   When saturation matrix crack spacing increases, the initial composite strain decreases, the initial tangent modulus increases and the transition stress for interface debonding and initial fiber broken fraction remain the same;

(5)   When the fiber strength increases, the initial composite strain and fiber broken fraction decrease and the initial tangent composite modulus and transition stress for interface debonding remains the same.

Conflicts of Interest: The authors declare no conflict of interest.

References

1.   Naslain, R. Design, Preparation and properties of non-oxide CMCs for application in engines and nuclear reactors: An overview. *Compos. Sci. Technol.* **2004**, *64*, 155–170. [CrossRef]

2.   Li, L.B.; Reynaud, P.; Fantozzi, G. Cyclic-dependent damage evolution in self-healing woven SiC/[Si-B-C] ceramic-matrix composites at elevated temperatures. *Materials* **2020**, *13*, 1478. [CrossRef] [PubMed]

3.   Ruggles-Wrenn, M.B.; Christensen, D.T.; Chamberlain, A.L.; Lane, J.E.; Cook, T.S. Effect of frequency and environment on fatigue behavior of a CVI SiC/SiC ceramic matrix composite at 1200 °C. *Compos. Sci. Technol.* **2011**, *71*, 190–196. [CrossRef]

4.   Li, P.; Wang, B.; Zhen, W.; Jiao, G. Tensile loading/unloading stress–strain behavior of 2D-SiC/SiC composites. *Fuhe Cailiao Xuebao/acta Materiae Compositae Sinica* **2014**, *31*, 676–682.

5.   Liu, Y. Study on damage failure mechanism of SiC/SiC ceramic matrix composites. Master Thesis, Harbin Institute of Technology, Harbin, China, 2019.

6.   Guo, S.; Kagawa, Y. Tensile fracture behavior of continuous SiC fiber-reinforced SiC matrix composites at elevated temperatures and correlation to in situ constituent properties. *J. Euro Ceram. Soc.* **2002**, *22*, 2349–2356. [CrossRef]

7.   Morscher, G.N. Modal acoustic emission of damage accumulation in a woven SiC/SiC composite. *Compos. Sci Technol.* **1999**, *59*, 687–697. [CrossRef]

8.   Marsili, R.; Rossi, G.; Speranzini, E. Fibre bragg gratings for the monitoring of wooden structures. *Materials* **2018**, *11*, 7. [CrossRef]

9.   Morscher, G.N.; Pujar, V.V. Design guidance for in-plane mechanical properties of SiC fiber-reinforced melt-infiltrated SiC composites. *Int J. Appl Ceram. Technol* **2009**, *6*, 151–163. [CrossRef]

10.   Marshall, D.B.; Cox, B.N.; Evans, A.G. The mechanics of matrix cracking in brittle-matrix fiber composites. *Acta Metall.* **1985**, *33*, 2013–2021. [CrossRef]

11.   Zok, F.W.; Spearing, S.M. Matrix crack spacing in brittle matrix composites. *Acta Metall. Mater.* **1992**, *40*, 2033–2043. [CrossRef]

12.   Curtin, W.A. Multiple matrix cracking in brittle matrix composites. *Acta Metall. Mater.* **1993**, *41*, 1369–1377. [CrossRef]

13.   Evans, A.G. Design and life prediction issues for high-temperature engineering ceramics and their composites. *Acta Mater.* **1997**, *45*, 23–40. [CrossRef]

14. McNulty, J.C.; Zok, F.W. Low-cycle fatigue of Nicalon-fiber-reinforced ceramic composites. *Compos. Sci. Technol.* **1999**, *59*, 1597–1607. [CrossRef]

15. Naslain, R.; Lamon, J.; Pailler, R.; Bourrat, X.; Guette, A.; Langlais, F. Micro/minicomposites: A useful approach to the design and development of non-oxide CMCs. *Compos. Part A* **1999**, *30*, 537–547. [CrossRef]

16. Goto, K.; Kagawa, Y. Fracture behavior and toughness of a plain-woven SiC fiber-reinforced SiC matrix composite. *Mater. Sci. Eng A.* **1996**, *211*, 72–81. [CrossRef]

17. Meyer, P.; Wass, A.M. Experimental results on the elevated temperature tensile response of SiC/SiC ceramic matrix notched composites. *Compos. Part B* **2018**, *143*, 269–281. [CrossRef]

18. Li, L.B.; Song, Y.; Sun, Y. Modeling the tensile behavior of unidirectional C/SiC ceramic-matrix composites. *Mech Compos. Mater.* **2013**, *49*, 659–672. [CrossRef]

19. Li, L.B.; Song, Y.; Sun, Y. Modeling the tensile behavior of cross-ply C/SiC ceramic-matrix composites. *Mech Compos. Mater.* **2015**, *51*, 359–376. [CrossRef]

20. Li, L.B. Modeling the monotonic and cyclic tensile stress–strain behavior of 2D and 2.5D woven C/SiC ceramic-matrix composites. *Mech Compos. Mater.* **2018**, *54*, 165–178. [CrossRef]

21. Curtin, W.A. Theory of mechanical properties of ceramic-matrix composites. *J. Am. Ceram. Soc.* **1991**, *74*, 2837–2845. [CrossRef]

22. Li, L.B. Assessment of the interfacial properties from fatigue hysteresis loss energy in ceramic-matrix composites with different fiber preforms at room and elevated temperatures. *Mater. Sci. Eng. A* **2014**, *613*, 17–36.

23. Domergue, J.C.; Vagaggini, E.; Evans, A.G. Relationships between hysteresis measurements and the constituent properties of ceramic matrix composites: II, Experimental studies on unidirectional materials. *J. Am. Ceram. Soc.* **1995**, *78*, 2721–2731. [CrossRef]

24. Li, L.B. Modeling matrix fracture in fiber-reinforced ceramic-matrix composites with different fiber preforms. *Text. Res. J.* **2020**, *90*, 909–924. [CrossRef]

25. Guo, S.Q.; Kagawa, Y.; Tanaka, Y.; Masuda, C. Microstructure and role of outermost coating for tensile strength of SiC fiber. *Acta Mater.* **1998**, *46*, 4941–4954. [CrossRef]